New Journal of Physics
The open access journal for physics

Lasing and antibunching of optical phonons in semiconductor double quantum dots

R Okuyama[1,3], **M Eto**[1] **and T Brandes**[2]

[1] Faculty of Science and Technology, Keio University, Yokohama 223-8522, Japan
[2] Institut für Theoretische Physik, Technische Universität Berlin, D-10623 Berlin, Germany
E-mail: rokuyama@rk.phys.keio.ac.jp

New Journal of Physics **15** (2013) 083032 (27pp)
Received 9 May 2013
Published 13 August 2013
Online at http://www.njp.org/
doi:10.1088/1367-2630/15/8/083032

Abstract. We theoretically propose optical phonon lasing in a double quantum dot (DQD) fabricated on a semiconductor substrate. No additional cavity or resonator is required. An electron in the DQD is found to be coupled to only two longitudinal optical phonon modes that act as a natural cavity. When the energy level spacing in the DQD is tuned to the phonon energy, the electron transfer is accompanied by the emission of the phonon modes. The resulting non-equilibrium motion of electrons and phonons is analyzed by the rate equation approach based on the Born–Markov–Secular approximation. We show that lasing occurs for pumping the DQD via electron tunneling at a rate much larger than the phonon decay rate, whereas phonon antibunching is observed in the opposite regime of slow tunneling. Both effects disappear by an effective thermalization induced by the Franck–Condon effect in a DQD fabricated in a suspended carbon nanotube with strong electron–phonon coupling.

[3] Author to whom any correspondence should be addressed.

Contents

1. Introduction

In conventional lasers, two-level systems couple to a single mode of photon in a cavity. The pumping of electrons to the upper level results in light amplification through the stimulated emission of radiation. Recently, lasing was reported for a single atom in a cavity, which is called a microlaser [1]. Such a system is being intensively studied in the context of cavity quantum electrodynamics (QED) [2], which also works as a single-photon source to produce antibunched photons [3].

Quantum dots are electrically tunable two-level systems. The cavity QED using a quantum dot has a potential for wider application to quantum information processing [4] as well as the single-photon source [5]. When the quantum dot is connected to an external circuit, the electronic state in the quantum dot can be controlled by the electric current. The microlaser was realized in the so-called circuit QED, in which a superconducting quantum dot in a circuit is coupled to a microwave resonator [6]. In this case, pumping is realized using the superconducting circuit. The electric current drives the lasing when level spacing is tuned to the microwave energy [7–11].

In this work, we theoretically examine the transport through a semiconductor double quantum dot (DQD) in the presence of electron–optical-phonon coupling and propose phonon lasing without a cavity or resonator. The electron–phonon interaction in quantum dots reveals

itself in the transport phenomenon, which was investigated in various contexts until now. For DQDs fabricated in InAs nanowire and graphene, an interference pattern of electric current was observed as a function of level spacing in the DQDs, which is ascribable to the emission of acoustic phonons [12]. It is the Dicke-type interference between two transport processes in which a longitudinal acoustic (LA) phonon is emitted in one dot or another [13]. In a single quantum dot fabricated in a suspended carbon nanotube (CNT), the Franck–Condon blockade was reported [14, 15]. Owing to the strong electron–phonon interaction in the CNT, the electric transport is accompanied by lattice distortion, which results in the current suppression under a small bias voltage [16]. This is the manifestation of the Franck–Condon effect in the electric transport, which was originally known in the optical absorption of molecules [17]. Regarding the study of optical phonons, Amaha and Ono observed phonon-assisted transport through a DQD. The current is markedly enhanced when the level spacing in the DQD is tuned to an integer multiple of the energy of longitudinal optical (LO) phonons in the semiconductor substrate [18].

In this paper, we show LO-phonon lasing in phonon-assisted transport through a DQD. First, we show that a DQD effectively couples to only two LO phonon modes. The phonon modes do not diffuse and act as a natural cavity since the optical phonons have a flat dispersion relation. Thus, our laser does not require a cavity or resonator. The pumping to the upper level is realized by an electric current through the DQD under a finite bias voltage, in a similar manner to the microlaser in the circuit QED [6]. Thus, the pumping rate is determined by the tunneling rate between the DQD and leads, $\Gamma_{L,R}$. The amplified LO phonons occasionally escape from the 'cavity' by decaying into the so-called daughter phonons [19] that can be observed externally (see section 6). When the pumping rate $\Gamma_{L,R}$ is much larger than the phonon decay rate $\Gamma_{\rm ph}$, the stimulated emission of phonons, i.e. phonon lasing, takes place. We proposed a basic idea of optical phonon lasing in our previous letter [20]. In this paper, we present further comprehensive discussion on phonon lasing and address the possible experimental realization.

We also find phonon antibunching in the same system if the pumping rate $\Gamma_{L,R}$ is smaller than $\Gamma_{\rm ph}$. In this situation, the phonon emission is regularized by single-electron transport through the DQD. We emphasize that the phonon statistics can be changed by electrically tuning the tunnel coupling between DQD and leads. Note that LO-phonon-assisted transport through a DQD was theoretically studied by Gnodtke *et al* [21]. We also note that the lasing of acoustic phonons was studied in semiconductor superlattices, which work as a cavity to confine acoustic phonons [22]. The acoustic phonon laser using a single quantum dot was theoretically proposed by optical pumping [23] and by spin-dependent transport [24].

The electron–phonon coupling in DQDs fabricated in CNTs is much stronger than the electron–optical-phonon coupling in DQDs made in GaAs substrate, as we discuss in section 2. Both phonon lasing and antibunching are spoilt by phonon thermalization via the Franck–Condon effect in the former case. In electric transport, the number of electrons in the DQD fluctuates, which is accompanied by lattice distortion and thus the creation of bunched phonons. We show that this effect is negligible in a weak coupling case of semiconductor-based DQDs but surpasses lasing and antibunching in a strong coupling case of CNTs[4]. We also show that the strong electron–phonon coupling brings about Franck–Condon blockade in a DQD with finite bias voltages, as in the case of single quantum dots [14–16].

[4] The coupling to photons in a cavity corresponds to the weak coupling case, with a dimensionless coupling constant $\lambda \sim 10^{-4}$ in [1] and 10^{-2} in [6], in equation (7).

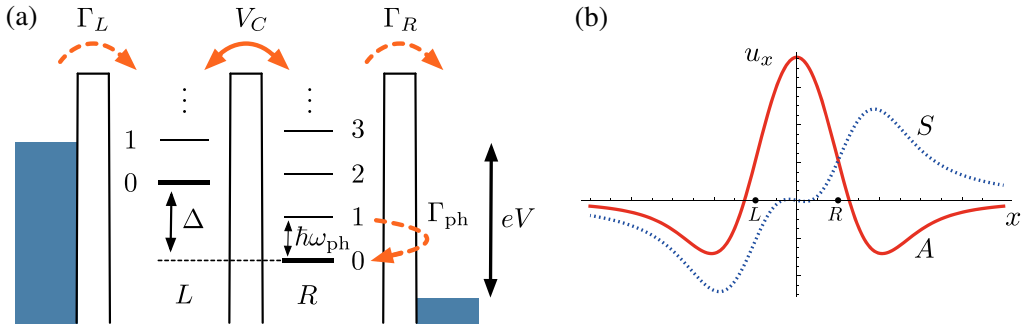

Figure 1. (a) Model for a DQD coupled to LO phonons. The bias voltage V is applied between external leads. The spacing Δ between the energy levels in dots L and R is electrically tunable. When Δ matches an integer (ν) multiple of the phonon energy $\hbar\omega_{\rm ph}$, the electronic state $|L\rangle_{\rm e}$ with n phonons is coherently coupled to $|R\rangle_{\rm e}$ with $(n+\nu)$ phonons. (b) The phonon mode functions $\boldsymbol{u}_{\rm S,A}(\boldsymbol{r})$ along a line through the centers of quantum dots located at $x = \pm\mathcal{R}$, when the electron distributions, $|\psi_L(\boldsymbol{r})|^2$ and $|\psi_R(\boldsymbol{r})|^2$, are spherical with radius $\mathcal{R}$. The x-component of $\boldsymbol{u}(x, 0, 0)$ is shown for S(A)-phonons which couple (anti-)symmetrically to the DQD. Note that u_x is an odd (even) function of x for S (A)-phonons since the induced charge is proportional to $\nabla \cdot \boldsymbol{u}(\boldsymbol{r})$.

This paper is organized as follows. In section 2, we explain our model and calculation method. Starting from the microscopic electron–optical-phonon interaction, we show that only two phonon modes, S- and A-phonons, are coupled to an electron in the DQD. The effective Hamiltonian is then derived in terms of the phonon modes. Based on the Born–Markov–Secular (BMS) approximation, we obtain the rate equation for the non-equilibrium dynamics of electrons and phonons in the DQD under a finite bias. In section 3, we take into account A-phonons and disregard S-phonons. We examine the electron transport accompanied by the phonon emission. This results in phonon lasing or antibunching in the weak coupling case, whereas it brings about phonon thermalization in the strong coupling case. These different situations are elucidated by the analytical solution of the rate equation as well as the numerical studies. In section 4, S-phonons are examined without A-phonons. S-phonons do not contribute to the phonon-assisted tunneling in the DQD, in contrast to A-phonons, and hence they are irrelevant to phonon lasing and antibunching. We examine the Franck–Condon blockade under a finite bias by coupling to S-phonons as well as A-phonons. Section 5 is devoted to the investigation of general situations in the presence of both A- and S-phonons. We show that S-phonons do not disturb the lasing or antibunching of A-phonons. In section 6, we discuss the validity of our theory and address possible experimental realizations to observe phonon lasing and antibunching. Finally, we present our conclusions in section 7.

2. Model and calculation method

2.1. Phonon modes coupled to a double quantum dot and effective Hamiltonian

Figure 1(a) depicts our model of a DQD embedded in a semiconductor substrate, in which two single-level quantum dots, L and R, are connected by tunnel coupling $V_{\rm C}$. The energy levels, ε_L and ε_R, are electrically tunable. We choose $\varepsilon_R = -\varepsilon_L$ and denote the level spacing $\varepsilon_L - \varepsilon_R$

by Δ. We assume that the total number of electrons in the DQD is restricted to one or zero due to Coulomb blockade. The electron couples to LO phonons of energy $\hbar\omega_{\rm ph}$ in the substrate by the Fröhlich interaction. Our system Hamiltonian is $\mathcal{H} = \mathcal{H}_{\rm e} + \mathcal{H}_{\rm ph} + \mathcal{H}_{\rm ep}$,

$$\mathcal{H}_{\rm e} = \frac{\Delta}{2}(n_L - n_R) + V_{\rm C}(d_L^\dagger d_R + d_R^\dagger d_L), \tag{1}$$

$$\mathcal{H}_{\rm ph} = \hbar\omega_{\rm ph}\sum_{\boldsymbol{q}} N_{\boldsymbol{q}}, \tag{2}$$

$$\mathcal{H}_{\rm ep} = \sum_{\alpha=L,R}\sum_{\boldsymbol{q}} M_{\alpha,\boldsymbol{q}}(a_{\boldsymbol{q}} + a_{-\boldsymbol{q}}^\dagger)n_\alpha \tag{3}$$

using creation (annihilation) operators $d_\alpha^\dagger$ (d_α) for an electron in dot α and $a_{\boldsymbol{q}}^\dagger$ ($a_{\boldsymbol{q}}$) for a phonon with wavevector $\boldsymbol{q}$. $n_\alpha = d_\alpha^\dagger d_\alpha$ and $N_{\boldsymbol{q}} = a_{\boldsymbol{q}}^\dagger a_{\boldsymbol{q}}$ are the number operators. The spin index is omitted for electrons. The coupling constant is given by

$$M_{\alpha,\boldsymbol{q}} = \sqrt{\frac{e^2\hbar\omega_{\rm ph}}{2\mathcal{V}}\left[\frac{1}{\epsilon(\infty)} - \frac{1}{\epsilon(0)}\right]}\frac{1}{q}\int \mathrm{d}\boldsymbol{r}|\psi_\alpha(\boldsymbol{r})|^2 \mathrm{e}^{\mathrm{i}\boldsymbol{q}\cdot\boldsymbol{r}}, \tag{4}$$

where $\epsilon(\infty)$ ($\epsilon(0)$) is the dielectric constant at high (low) frequency, $\mathcal{V}$ is the volume of substrate and $\psi_\alpha(\boldsymbol{r})$ is the electron wavefunction in dot α of radius $\mathcal{R}$. The LO phonons only around the Γ point, such as $|\boldsymbol{q}| \lesssim 1/\mathcal{R}$, are coupled to the DQD because of an oscillating factor in the integral over $|\psi_\alpha(\boldsymbol{r})|^2$. This fact justifies the dispersionless phonons in $\mathcal{H}_{\rm ph}$. We assume equivalent quantum dots L and R, whence $M_{R,\boldsymbol{q}} = M_{L,\boldsymbol{q}}\,\mathrm{e}^{\mathrm{i}\boldsymbol{q}\cdot\boldsymbol{r}_{LR}}$ with $\boldsymbol{r}_{LR}$ being a vector joining their centers.

In $\mathcal{H}_{\rm ep}$, an electron in dot α couples to a single mode of phonon described by

$$a_\alpha = \frac{\sum_{\boldsymbol{q}} M_{\alpha,\boldsymbol{q}} a_{\boldsymbol{q}}}{(\sum_{\boldsymbol{q}} |M_{\alpha,\boldsymbol{q}}|^2)^{1/2}}. \tag{5}$$

We perform a unitary transformation for phonons from $a_{\boldsymbol{q}}$ to S- and A-phonon modes:

$$a_{\rm S} = \frac{a_L + a_R}{\sqrt{2 + (\mathcal{S} + \mathcal{S}^*)}}, \quad a_{\rm A} = \frac{a_L - a_R}{\sqrt{2 - (\mathcal{S} + \mathcal{S}^*)}} \tag{6}$$

and others orthogonal to $a_{\rm S}$ and $a_{\rm A}$, where $\mathcal{S}$ is the overlap integral between a_L and a_R phonons in equation (5).[5] Since the phonon modes other than S- and A-phonons are decoupled from the DQD, they can be safely disregarded in the electron transport through the DQD. Hence, we obtain the effective Hamiltonian

$$H = \mathcal{H}_{\rm e} + \hbar\omega_{\rm ph}\left[N_{\rm S} + \lambda_{\rm S}(a_{\rm S} + a_{\rm S}^\dagger)(n_L + n_R)\right] + \hbar\omega_{\rm ph}\left[N_{\rm A} + \lambda_{\rm A}(a_{\rm A} + a_{\rm A}^\dagger)(n_L - n_R)\right], \tag{7}$$

where $N_{\rm S} = a_{\rm S}^\dagger a_{\rm S}$ and $N_{\rm A} = a_{\rm A}^\dagger a_{\rm A}$, with dimensionless coupling constants

$$\lambda_{\rm S/A} = \frac{1}{2\hbar\omega_{\rm ph}}\left(\sum_{\boldsymbol{q}} |M_{L,\boldsymbol{q}} \pm M_{R,\boldsymbol{q}}|^2\right)^{1/2}. \tag{8}$$

The mode functions for S- and A-phonons are shown in figure 1(b) along a line through the centers of the quantum dots. The definition and calculation of the mode functions are given

[5] The overlap integral, $\mathcal{S} = {}_{\rm ph}\langle L|R\rangle_{\rm ph} = {}_{\rm ph}\langle 0|a_L a_R^\dagger|0\rangle_{\rm ph} = [a_L, a_R^\dagger]$, is evaluated in appendix A.

in appendix A. Since the phonons are dispersionless, they do not diffuse and act as a cavity including the DQD.[6] A-phonons play a crucial role in the phonon-assisted tunneling between the quantum dots and thus in the phonon lasing, as discussed below, whereas S-phonons do not since it couples to the *total* number of electrons in the DQD, $n_L + n_R$. Both phonons are relevant to the Franck–Condon effect.

Our Hamiltonian H in equation (7) is applicable to DQDs fabricated in a semiconductor substrate, where $\hbar\omega_{\rm ph} = 36\,{\rm meV}$ and $\lambda_{\rm S,A} = 0.1$–0.01 for $\mathcal{R} = 10$–$100\,{\rm nm}$ in GaAs. It also describes a DQD in a suspended CNT when an electron couples to a vibron, longitudinal stretching mode with $\hbar\omega_{\rm ph} \sim 1\,{\rm meV}$, $\lambda_{\rm A} \gtrsim 1$ and $\lambda_{\rm S} = 0$ in experimental situations [14, 15], as shown in appendix B.

2.2. Rate equation in energy eigenbasis

The DQD is connected to external leads L and R in series, which enables electronic pumping by the electric current under a finite bias. The tunnel coupling between lead L and dot L is denoted by Γ_L and that between lead R and dot R by Γ_R. We also introduce the phonon decay rate $\Gamma_{\rm ph}$ to take into account natural decay of LO phonons into the so-called daughter phonons due to lattice anharmonicity [19]. We describe the dynamics of the DQD-phonon density matrix ρ using a Markovian master equation

$$\dot{\rho} = -\frac{\rm i}{\hbar}[H, \rho] + \mathcal{L}_{\rm e}\rho + \mathcal{L}_{\rm ph}\rho, \tag{9}$$

where $\mathcal{L}_{\rm e}$ and $\mathcal{L}_{\rm ph}$ describe the electron tunneling between the DQD and leads and the phonon decay, respectively. $\mathcal{L}_{\rm e}$ is written as

$$\begin{aligned}\mathcal{L}_{\rm e}\rho = \sum_{\alpha=L,R;i,j} \frac{\Gamma_\alpha}{2}\Big[& f_\alpha(\epsilon_i - \epsilon_j)\Big(|i\rangle\langle i|d_\alpha^\dagger|j\rangle\langle j|\rho d_\alpha + d_\alpha^\dagger\rho|j\rangle\langle j|d_\alpha|i\rangle\langle i| \\ & -\rho|j\rangle\langle j|d_\alpha|i\rangle\langle i|d_\alpha^\dagger - d_\alpha|i\rangle\langle i|d_\alpha^\dagger|j\rangle\langle j|\rho\Big) \\ & +\bar{f}_\alpha(\epsilon_i - \epsilon_j)\Big(|j\rangle\langle j|d_\alpha|i\rangle\langle i|\rho d_\alpha^\dagger + d_\alpha\rho|i\rangle\langle i|d_\alpha^\dagger|j\rangle\langle j| \\ & -\rho|i\rangle\langle i|d_\alpha^\dagger|j\rangle\langle j|d_\alpha - d_\alpha^\dagger|j\rangle\langle j|d_\alpha|i\rangle\langle i|\rho\Big)\Big]\end{aligned} \tag{10}$$

with $|i\rangle$ and ϵ_i being an eigenstate of H and the corresponding energy eigenvalue and $f_\alpha(\epsilon)$ [$\bar{f}_\alpha(\epsilon) = 1 - f_\alpha(\epsilon)$] being the Fermi distribution function for electrons (holes) in lead α [25]. The Fermi levels in leads L and R are given by $\mu_L = eV/2$ and $\mu_R = -eV/2$, respectively, with bias voltage V between the leads.

In the limit of large bias voltage, $\mathcal{L}_{\rm e}$ is reduced to

$$\mathcal{L}_{\rm e}\rho = (\Gamma_L\mathcal{D}[d_L^\dagger] + \Gamma_R\mathcal{D}[d_R])\rho, \tag{11}$$

where $\mathcal{D}[A]\rho = A\rho A^\dagger - \frac{1}{2}\{\rho, A^\dagger A\}$ is a Lindblad dissipator. In this case, an electron tunnels into dot L from lead L with tunneling rate Γ_L and tunnels out from dot R to lead R with Γ_R in one direction. We examine this situation in the main part of this paper. With finite bias voltages,

[6] If a weak quadratic dispersion around the Γ point is taken into account, the phonon modes are scattered by the rate of $\partial^2\omega_{\rm ph}/\partial q^2|_{q=0}/\mathcal{R}^2$, which is smaller than the decay rate $\Gamma_{\rm ph}$ of LO phonons by two orders of magnitude in GaAs quantum dots with $\mathcal{R} = 10$–$100\,{\rm nm}$.

equation (10) is evaluated in sections 3.3 and 4.2, where electron tunneling takes place in both directions unless eV is far beyond the temperature T.

The phonon dissipator $\mathcal{L}_{\rm ph}$ is given by

$$\mathcal{L}_{\rm ph}\rho = \Gamma_{\rm ph}(\mathcal{D}[a_{\rm S}] + \mathcal{D}[a_{\rm A}])\rho \tag{12}$$

on the assumption that the temperature T in the substrate is much smaller than $\hbar\omega_{\rm ph}$, and daughter phonons immediately escape from the surroundings of DQD.

In the following, we adopt the BMS approximation [26] to equation (9). We diagonalize the Hamiltonian H in equation (7) and set up the rate equation in the energy eigenbasis,

$$\dot{P}_i = \sum_j L_{ij} P_j \tag{13}$$

for probability P_i to find the system in eigenstate $|i\rangle$. Here, $L_{ij} = \langle i|[(\mathcal{L}_{\rm e} + \mathcal{L}_{\rm ph})|j\rangle\langle j|]|i\rangle$. The solution of equation (13) with $\dot{P}_i = 0$ determines the steady-state properties. The condition to justify the BMS approximation will be given in section 6.

3. Lasing and antibunching of A-phonons

In this section, we examine A-phonons, disregarding S-phonons, by fixing at $\lambda_{\rm S} = 0$. The results in this section are not modified by a finite coupling to S-phonons, as seen in section 5.

3.1. Phonon-assisted transport and phonon lasing

First, we present our numerical results in the case of $\Gamma_{L,R} \gg \Gamma_{\rm ph}$. We consider the limit of large bias voltage. Figure 2(a) shows the current I through the DQD as a function of level spacing Δ, with $\lambda_{\rm A} = 0.1$ (solid line) and 1 (dotted line). Beside the main peak at $\Delta = 0$, we observe subpeaks at $\Delta = \Delta_\nu \simeq \nu\hbar\omega_{\rm ph}$ ($\nu = 1, 2, 3, \ldots$) due to the phonon-assisted tunneling[7]. At the νth subpeak, electron transport through DQD is accompanied by the emission of ν phonons. As a result, the phonon number is markedly enhanced at the subpeaks, as shown in figure 2(b), in both cases of $\lambda_{\rm A} = 0.1$ and 1. However, the physics is very different for the two cases, as we will show below.

For $\lambda_{\rm A} = 0.1$ and $\Delta = \Delta_\nu$, the electronic state $|L\rangle_{\rm e}$ with n phonons is coherently coupled to $|R\rangle_{\rm e}$ with $(n+\nu)$ phonons [27], similarly to cavity QED systems, if the lattice distortion is neglected. To examine the amplification of A-phonons, we calculate the phonon autocorrelation function

$$g_{\rm A}^{(2)}(\tau) = \frac{\langle : N_{\rm A}(0)N_{\rm A}(\tau) : \rangle}{\langle N_{\rm A}\rangle^2}. \tag{14}$$

The numerator includes the normal product $: N_{\rm A}(0)N_{\rm A}(\tau) := a_{\rm A}^\dagger(0)a_{\rm A}^\dagger(\tau)a_{\rm A}(\tau)a_{\rm A}(0)$. $g_{\rm A}^{(2)}(\tau)$ is proportional to the probability of phonon emission at time τ on the condition that a phonon is emitted at time 0 [28, 29]. A value of $g_{\rm A}^{(2)}(0) = 1$ indicates a *Poisson* distribution of phonons which is a criterion of phonon lasing, whereas $g_{\rm A}^{(2)}(0) < 1$ ($g_{\rm A}^{(2)}(0) > 1$) represents the phonon antibunching (bunching). We thus find phonon lasing at the current subpeaks in figure 2(c) in the case of $\lambda_{\rm A} = 0.1$ (solid line).

[7] Δ_ν is not exactly equal to $\nu\hbar\omega_{\rm ph}$ in the presence of tunnel coupling $V_{\rm C}$ between the quantum dots.

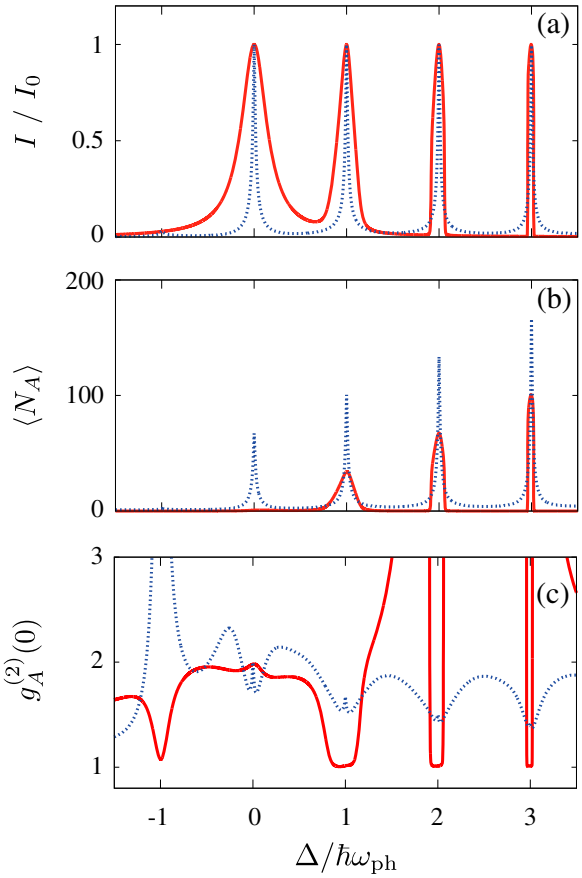

Figure 2. (a) Electric current through the DQD, (b) A-phonon number $\langle N_{\rm A}\rangle$, and (c) its autocorrelation function $g_{\rm A}^{(2)}(0)$ in the large bias-voltage limit, as a function of level spacing Δ in the DQD. The dimensionless electron–phonon coupling constants are $\lambda_{\rm A} = 0.1$ (solid lines) or 1 (dotted lines), and $\lambda_{\rm S} = 0$. In (a), $I_0 = e\Gamma_R/(2+\Gamma_R/\Gamma_L)$ is the current at $\Delta = 0$ in the absence of electron–phonon coupling. $\Gamma_L = \Gamma_R = 100\ \Gamma_{\rm ph}$ and $V_{\rm C} = 0.1\hbar\omega_{\rm ph}$.

When $\lambda_{\rm A} = 1$, the strength of the electron–phonon interaction is comparable with the phonon energy. In this case, the lattice distortion by the Franck–Condon effect seriously disturbs the above mentioned coherent coupling between an electron and phonons in the DQD and, as a result, suppresses the phonon lasing. Indeed, $g_{\rm A}^{(2)}(0) > 1$ at the current subpeaks, indicating phonon bunching.

To compare the two situations in detail, we present the number distribution of A-phonons in figures 3(a) and (b) at the current main peak and subpeaks. In the case of $\lambda_{\rm A} = 0.1$, a Poisson-like distribution emerges at the subpeaks, whereas a Bose distribution with effective temperature T^* is seen at the main peak. T^* is determined from the number of phonons $\langle N_{\rm A}\rangle$ in the stationary state as $1/[{\rm e}^{\hbar\omega_{\rm ph}/(k_{\rm B}T^*)} - 1] = \langle N_{\rm A}\rangle$. When $\lambda_{\rm A} = 1$, on the other hand, the distribution shows an intermediate shape between Poisson and Bose distributions at the subpeaks and the Bose distribution at the main peak.

In figures 4(a) and (b), we plot the autocorrelation function $g_{\rm A}^{(2)}(\tau)$ as a function of τ. In the case of $\lambda_{\rm A} = 0.1$, $g_{\rm A}^{(2)}(\tau) \simeq 1$, regardless of the time delay τ, which supports the

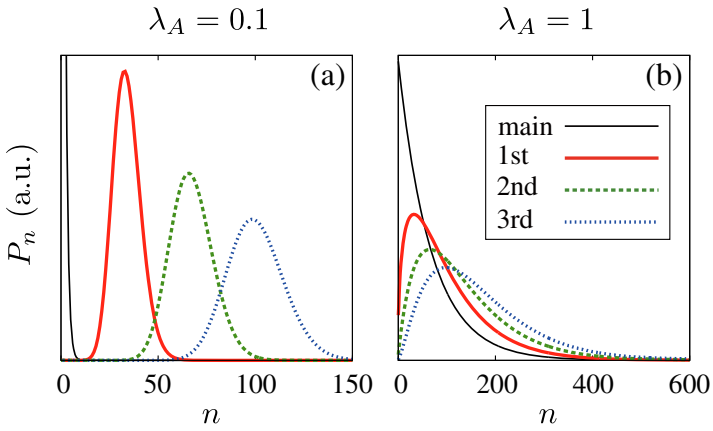

Figure 3. Number distribution of A-phonons at the current main peak ($\Delta = 0$) and subpeaks ($\Delta = \Delta_\nu \simeq \nu\hbar\omega_{\rm ph}$, $\nu = 1, 2, 3$) in figure 2(a). (a) $\lambda_{\rm A} = 0.1$ or (b) 1, and $\lambda_{\rm S} = 0$. The other parameters are the same as in figure 2.

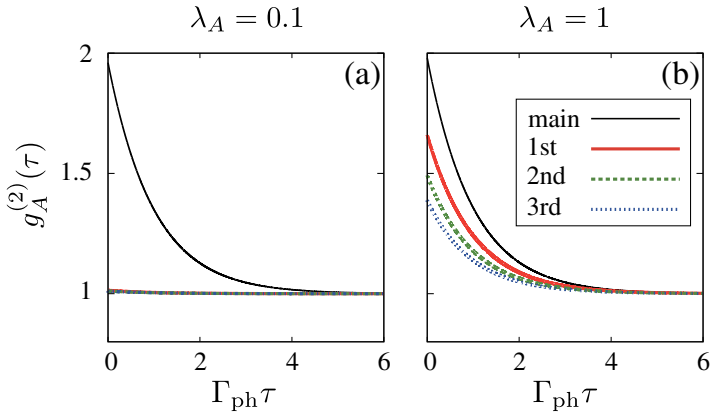

Figure 4. Autocorrelation function of A-phonons, $g_{\rm A}^{(2)}(\tau)$, at the current main peak ($\Delta = 0$) and subpeaks ($\Delta = \Delta_\nu \simeq \nu\hbar\omega_{\rm ph}$, $\nu = 1, 2, 3$) in figure 2(a). (a) $\lambda_{\rm A} = 0.1$ or (b) 1, and $\lambda_{\rm S} = 0$. The other parameters are the same as in figure 2. Note that the three lines for the current subpeaks are almost overlapped in (a).

phonon lasing at the current subpeaks. At the main peak, $g_{\rm A}^{(2)}(\tau) \simeq 1 + {\rm e}^{-\Gamma_{\rm ph}\tau}$. This is a character of thermal phonons with temperature T^*. When $\lambda_{\rm A} = 1$, we find intermediate behavior, $g_{\rm A}^{(2)}(\tau) \simeq 1 + \delta_\nu\, {\rm e}^{-\Gamma_{\rm ph}\tau}$ $(0 < \delta_\nu < 1)$, at the νth subpeak. This indicates that the phonons are partly thermalized by the Franck–Condon effect. For larger ν, the distribution is closer to the Poissonian with smaller δ_ν.

3.2. Competition between phonon lasing and Franck–Condon thermalization

To elucidate the competition between phonon lasing and thermalization by the Franck–Condon effect, we analyze the rate equation in equation (13), focusing on the current peaks in the large bias-voltage limit. We introduce polaron states $|L(R), n\rangle_{\rm eA}$ for an electron in dot L (R) and n

phonons with lattice distortion:

$$|L,n\rangle_{\mathrm{eA}} = |L\rangle_{\mathrm{e}} \otimes \mathcal{T}_{\mathrm{A}}|n\rangle_{\mathrm{A}}, \quad |R,n\rangle_{\mathrm{eA}} = |R\rangle_{\mathrm{e}} \otimes \mathcal{T}_{\mathrm{A}}^{\dagger}|n\rangle_{\mathrm{A}}, \tag{15}$$

where

$$\mathcal{T}_{\mathrm{A}} = \mathrm{e}^{-\lambda_{\mathrm{A}}(a_{\mathrm{A}}^{\dagger} - a_{\mathrm{A}})} \tag{16}$$

and its Hermitian conjugate $\mathcal{T}_{\mathrm{A}}^{\dagger}$ describes the shift of equilibrium position of the lattice when an electron stays in dots L and R. Note that the lattice distortion produces λ_{A}^2 extra phonons: ${}_{\mathrm{eA}}\langle\alpha,n|N_{\mathrm{A}}|\alpha,n\rangle_{\mathrm{eA}} = n + \lambda_{\mathrm{A}}^2$. When $\Delta = \Delta_{\nu}$ ($\simeq \nu\hbar\omega_{\mathrm{ph}}$), the eigenstates of Hamiltonian H are given by the zero-electron states $|0,n\rangle_{\mathrm{eA}} = |0\rangle_{\mathrm{e}} \otimes |n\rangle_{\mathrm{A}}$, bonding and anti-bonding states between the polarons,

$$|\pm,n\rangle_{\mathrm{eA}} = \frac{1}{\sqrt{2}}(|L,n\rangle_{\mathrm{eA}} \pm |R,n+\nu\rangle_{\mathrm{eA}}) \tag{17}$$

($n = 0, 1, 2, \ldots$), and polarons localized in dot R, $|R,n\rangle$ ($n = 0, 1, 2, \ldots, \nu-1$). This is a good approximation provided that $V_{\mathrm{C}} \ll \hbar\omega_{\mathrm{ph}}$. The rate equations for these states are

$$\begin{aligned}\dot{P}_{0,n} = {} & -\Gamma_L P_{0,n} + \sum_{m=0}^{\infty} \frac{\Gamma_R}{2} |{}_{\mathrm{A}}\langle n|\mathcal{T}_{\mathrm{A}}^{\dagger}|m+\nu\rangle_{\mathrm{A}}|^2 P_{\mathrm{mol},m} + \sum_{m=0}^{\nu-1} \Gamma_R |{}_{\mathrm{A}}\langle n|\mathcal{T}_{\mathrm{A}}^{\dagger}|m\rangle_{\mathrm{A}}|^2 P_{R,m} \\ & + \Gamma_{\mathrm{ph}}\left[(n+1)P_{0,n+1} - nP_{0,n}\right],\end{aligned} \tag{18}$$

$$\dot{P}_{\mathrm{mol},n} = -\frac{\Gamma_R}{2} P_{\mathrm{mol},n} + \sum_{m=0}^{\infty} \Gamma_L |{}_{\mathrm{A}}\langle n|\mathcal{T}_{\mathrm{A}}|m\rangle_{\mathrm{A}}|^2 P_{0,m} + \Gamma_{\mathrm{ph}}\left[\left(n+1+\frac{\nu}{2}\right)P_{\mathrm{mol},n+1} - \left(n+\frac{\nu}{2}\right)P_{\mathrm{mol},n}\right], \tag{19}$$

where $P_{\mathrm{mol},n} = P_{+,n} + P_{-,n}$ ($n = 0, 1, 2, \ldots$) and

$$\dot{P}_{R,n} = -\Gamma_R P_{R,n} + \Gamma_{\mathrm{ph}}\left[(n+1)P_{R,n+1} - nP_{R,n}\right], \tag{20}$$

with $P_{R,\nu} = P_{\mathrm{mol},0}/2$ ($n = 0, 1, 2, \ldots, \nu-1$). As shown in appendix C, these equations yield the current I and electron number in the DQD, $\langle n_{\mathrm{e}}\rangle = \langle n_L + n_R\rangle$, in terms of the number of polarons localized in dot R, $\langle\tilde{n}_R\rangle = \sum_{n=0}^{\nu-1} P_{R,n}$, as

$$I = e\Gamma_R \frac{1+\langle\tilde{n}_R\rangle}{2+\gamma}, \quad \langle n_{\mathrm{e}}\rangle = \frac{2-\gamma\langle\tilde{n}_R\rangle}{2+\gamma} \tag{21}$$

with $\gamma = \Gamma_R/\Gamma_L$. The number of A-phonons is given by

$$\langle N_{\mathrm{A}}\rangle = (\nu + 2\lambda_{\mathrm{A}}^2)\frac{I}{e\Gamma_{\mathrm{ph}}} + \lambda_{\mathrm{A}}^2\langle n_{\mathrm{e}}\rangle. \tag{22}$$

The first two terms in equation (22) indicate the emission of ν phonons by phonon-assisted tunneling (from dot L to dot R) and creation of $2\lambda_{\mathrm{A}}^2$ phonons by lattice distortion (with two tunnelings between the DQD and leads) per transfer of a single electron through the DQD. The last term describes the average number of polarons $\langle n_{\mathrm{e}}\rangle$ in the stationary state.

When $\Gamma_{L,R} \gg \Gamma_{\mathrm{ph}}$, we obtain

$$I = I_0 + \mathcal{O}(\Gamma_{\mathrm{ph}}/\Gamma_{L,R}), \tag{23}$$

where $I_0 = e\Gamma_R/(2+\gamma)$ is the current at the main peak in the absence of electron–phonon interaction, and

$$g_{\rm A}^{(2)}(0) = \frac{\nu + 4\lambda_{\rm A}^2}{\nu + 2\lambda_{\rm A}^2} + \mathcal{O}(\Gamma_{\rm ph}/\Gamma_{L,R}). \tag{24}$$

These explain the numerical results in figure 2 at the current subpeaks. The formula in equation (24) indicates $g_{\rm A}^{(2)}(0) \simeq 1$ (phonon lasing) for $\lambda_{\rm A}^2 \ll \nu$ and $g_{\rm A}^{(2)}(0) \simeq 2$ (thermalized phonons by the lattice distortion) for $\lambda_{\rm A}^2 \gg \nu$. In the latter case, the phonons follow Bose distribution with T^* to deduce $\langle N_{\rm A}\rangle$ in equation (22).

We comment on the peak width of the electric current in figure 2(a). The electron transfer around the νth current peak is dominated by the tunneling between polaron states $|L, n\rangle_{\rm eA}$ and $|R, n+\nu\rangle_{\rm eA}$ with $n \simeq \langle N_{\rm A}\rangle$. Thus, the peak width is determined by the effective tunnel coupling

$$\begin{aligned} W_\nu &= |_{\rm eA}\langle R, n+\nu|H_{\rm e}|L, n\rangle_{\rm eA}|_{n\simeq\langle N_{\rm A}\rangle} \\ &= \left|\frac{n!}{(n+\nu)!}(-2\lambda_{\rm A})^\nu {\rm e}^{-2\lambda_{\rm A}^2} L_n^\nu(4\lambda_{\rm A}^2) V_{\rm C}\right|_{n\simeq\langle N_{\rm A}\rangle} \end{aligned} \tag{25}$$

($\nu = 0, 1, 2, \ldots$), where $L_n^\nu(x)$ is the Laguerre polynomial[8]. The factor of ${\rm e}^{-2\lambda_{\rm A}^2}$ in equation (25) stems from the electron localization by dressing the phonons in forming the polarons. This explains the narrower subpeaks in the case of $\lambda_{\rm A} = 1$ than that of $\lambda_{\rm A} = 0.1$.

When $\lambda_{\rm A}^2 \ll 1$, equation (25) yields

$$W_\nu \simeq \sqrt{\langle N_{\rm A}\rangle + 1}\,\lambda_{\rm A}^\nu V_{\rm C}. \tag{26}$$

This is in quantitative accordance with the peak widths in the case of $\lambda_{\rm A} = 0.1$ (solid line in figure 2(a)).

3.3. Franck–Condon blockade

So far we have considered the large bias-voltage limit. In this subsection, we examine the case of finite bias voltages to elucidate the Franck–Condon blockade [14] in our system. Figures 5(a) and (b) show the electric current as a function of bias voltage V when the level spacing Δ is tuned to the main and subpeaks in figure 2(a). The electron–phonon coupling is (a) $\lambda_{\rm A} = 0.1$ and (b) 1. At the main peak ($\Delta = 0$) in case (a), the current is almost identical to I_0 in the large bias-voltage limit when $\mu_L = eV/2$ exceeds the interdot tunnel coupling $V_{\rm C}$. (The current vanishes when $eV/2 \lesssim V_{\rm C}$, reflecting the formation of bonding and antibonding orbitals at energy level $\pm V_{\rm C}$, from two orbitals at $\varepsilon_L = \varepsilon_R = 0$ in the DQD.) The influence of electron–phonon coupling is hardly observable. At the subpeaks ($\Delta = \Delta_\nu \simeq \nu\hbar\omega_{\rm ph}$, $\nu = 1, 2, 3$) in case (a), on the other hand, the current is suppressed at small V and it increases stepwise to the value in the large V limit. This is due to electron–phonon coupling, as explained below. The current suppression is much more prominent in the case of (b) with larger $\lambda_{\rm A}$. We observe the suppression even at the main peak in this case.

The reason for the current suppression is as follows. When an electron tunnels between the DQD and leads, the equilibrium position of the lattice is suddenly changed to form the polaron,

[8] In the absence of electron–phonon interaction, Δ-dependence of the current shows a peak at $\Delta = 0$. The peak width is given by the tunnel coupling $V_{\rm C}$ between the quantum dots (see equation (30)). In the presence of electron–phonon interaction, $V_{\rm C}$ is replaced by W_ν for the tunnel coupling between the polarons at the νth subpeak.

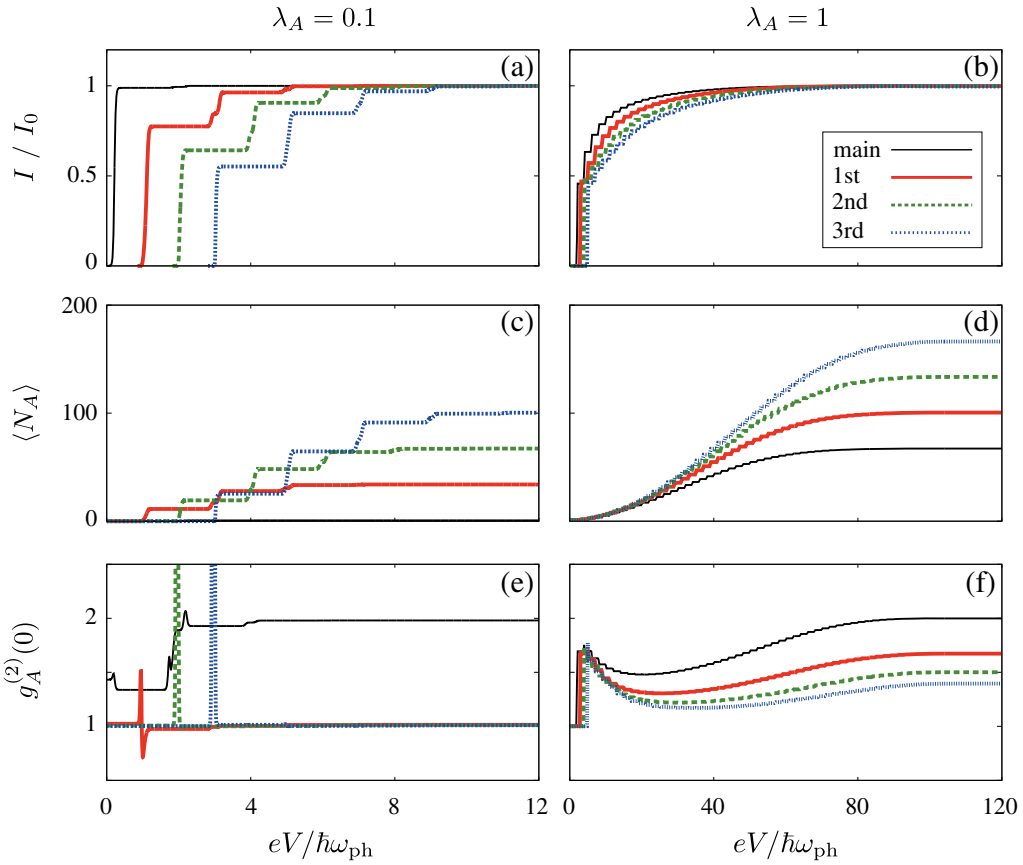

Figure 5. (a), (b) Electric current, (c), (d) A-phonon number $\langle N_{\rm A}\rangle$ and (e), (f) its autocorrelation function $g_{\rm A}^{(2)}(0)$, as a function of bias voltage V, at the current main peak ($\Delta = 0$) and subpeaks ($\Delta = \Delta_\nu \simeq \nu\hbar\omega_{\rm ph}$, $\nu = 1, 2, 3$) in figure 2(a). $\lambda_{\rm A} = 0.1$ in panels (a), (c) and (e), whereas $\lambda_{\rm A} = 1$ in panels (b), (d) and (f). $\lambda_{\rm S} = 0$ and $T = 0.01\hbar\omega_{\rm ph}$. The other parameters are the same as in figure 2.

$|L, n\rangle_{\rm eA}$ or $|R, n\rangle_{\rm eA}$, in equation (15). While all phonon states participate in polaron formation in the large bias-voltage limit, the phonon states are limited under finite bias voltages due to energy conservation. This weakens the tunnel coupling between the DQD and leads and also between the quantum dots, which is known as the Franck–Condon blockade. In figures 5(a) and (b), the current increases stepwise as $\mu_L = eV/2$ increases by $\hbar\omega_{\rm ph}$ because higher-energy states become accessible (Franck–Condon steps) and converges to $I = I_0$ in the large bias-voltage limit. The larger voltage is required to lift off the Franck–Condon blockade for larger $\lambda_{\rm A}$ [16].

Figures 5(c)–(f) show the phonon number and autocorrelation function $g_{\rm A}^{(2)}(0)$ as a function of V. The phonon number shows the Franck–Condon steps in both cases of (c) $\lambda_{\rm A} = 0.1$ and (d) 1. The autocorrelation function, on the other hand, is qualitatively different for the two cases. In figure 5(e) with $\lambda_{\rm A} = 0.1$, $g_{\rm A}^{(2)}(0) \simeq 1$ even at the first Franck–Condon step except for anomalous behavior around the beginning of the step. This indicates that phonon lasing is robust against the current suppression by the Franck–Condon blockade and hence it is observable under finite bias. In figure 5(f) with $\lambda_{\rm A} = 1$, $g_{\rm A}^{(2)}(0)$ changes slowly with V, reflecting V-dependence of the thermalization due to the Franck–Condon effect.

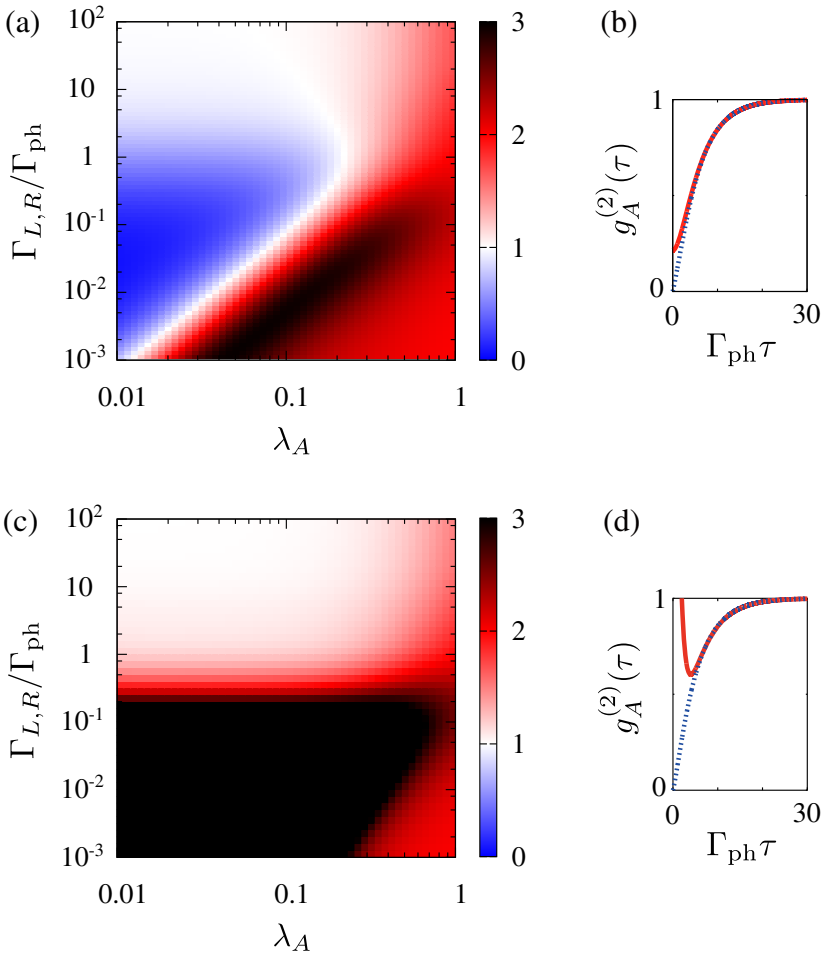

Figure 6. (a), (b) Color-scale plot of autocorrelation function of A-phonons, $g_{\rm A}^{(2)}(0)$, at the current subpeaks ($\Delta = \Delta_\nu \simeq \nu\hbar\omega_{\rm ph}$, $\nu = 1, 2$) in the large bias-voltage limit, in a plane of electron–phonon coupling $\lambda_{\rm A}$ and $\Gamma_{L,R}/\Gamma_{\rm ph}$. $\Gamma_L = \Gamma_R \equiv \Gamma_{L,R}$, $\lambda_{\rm S} = 0$, and $V_{\rm C} = 0.1\hbar\omega_{\rm ph}$. (c), (d) $g_{\rm A}^{(2)}(\tau)$ at $\lambda_{\rm A} = 0.05$ and $\Gamma_{L,R} = 0.1\ \Gamma_{\rm ph}$, as a function of τ (solid line). The autocorrelation function of electric current, $g_{\rm current}^{(2)}(\tau)$, is also shown by a dotted line. (a) and (b) are for the first current subpeak ($\nu = 1$), whereas (c) and (d) are for the second current subpeak ($\nu = 2$).

3.4. Phonon antibunching

In sections 3.1–3.3, we have restricted ourselves to the case of $\Gamma_{L,R} \gg \Gamma_{\rm ph}$ to examine phonon lasing. If tunnel coupling is tuned to be $\Gamma_{L,R} \lesssim \Gamma_{\rm ph}$, we observe another phenomenon, antibunching of A-phonons [30]. Figure 6(a) presents a color-scale plot of $g_{\rm A}^{(2)}(0)$ in the $\lambda_{\rm A}$–$(\Gamma_{L,R}/\Gamma_{\rm ph})$ plane when Δ is tuned to be at the first current subpeak ($\Delta = \Delta_1 \simeq \hbar\omega_{\rm ph}$). We assume that $\Gamma_L = \Gamma_R \equiv \Gamma_{L,R}$, $\lambda_{\rm S} = 0$, and large limit of bias voltage. At $\lambda_{\rm A} = 0.05$ and $\Gamma_{L,R}/\Gamma_{\rm ph} = 0.1$, for example, $g_{\rm A}^{(2)}(0) \ll 1$, representing a strong antibunching of phonons. This is because the phonon emission is regularized by the electron transport through the DQD.

In figure 6(b), we plot the autocorrelation function of the electric current

$$g^{(2)}_{\rm current}(\tau) = \frac{\langle : n_R(0) n_R(\tau) : \rangle}{\langle n_R \rangle^2}, \tag{27}$$

where n_R is the electron number in dot R. It fulfill $g^{(2)}_{\rm current}(0) = 0$, indicating the antibunching of electron transport, since dot R is empty just after the electron tunnels out [29]. Remarkably, $g^{(2)}_{\rm A}(\tau)$ almost coincides with $g^{(2)}_{\rm current}(\tau)$. When $\Gamma_{L,R} \ll \Gamma_{\rm ph}$, the emitted phonon escapes from the natural cavity soon after the electron tunneling between the quantum dots. Thus, the stimulated emission for the lasing does not take place.

At strong couplings of $\lambda_{\rm A} \gtrsim 1$, neither phonon antibunching nor phonon lasing can be observed because of effective phonon thermalization due to the Franck–Condon effect. More than one phonon is created by the polaron formation, which spoils the regularized phonon emission by single electron tunneling and results in phonon bunching.

Even with small $\lambda_{\rm A}$, bunched phonons are emitted if $\Gamma_{L,R}/\Gamma_{\rm ph}$ is too small. Then the number of phonons created by the tunneling is exceeded by that accompanied by the polaron staying in dot R (the first two terms are much smaller than the last term in equation (22)), as discussed in appendix (C.4.). The analytical expression of $g^{(2)}_{\rm A}(0)$ is also given for $\Gamma_{L,R} \ll \Gamma_{\rm ph}$ in the appendix.

Figure 6(c) shows a color-scale plot of $g^{(2)}_{\rm A}(0)$ when Δ is tuned to be at the second current subpeak ($\Delta = \Delta_2 \simeq 2\hbar\omega_{\rm ph}$). The antibunching does not occur even when $\Gamma_{L,R} \ll \Gamma_{\rm ph}$ because two phonons are emitted simultaneously by electron tunneling, which are bunched to each other.

4. Franck–Condon effect of S-phonons

In this section, we examine S-phonons and disregard A-phonons with $\lambda_{\rm A} = 0$.

4.1. Franck–Condon thermalization

We begin with the large bias-voltage limit. The electric current has a single-peaked structure as a function of Δ (Lorentzian with center at $\Delta = 0$ and width of $V_{\rm C}\sqrt{2+\gamma}$, as will be seen in equation (30)). We do not observe subpeaks at $\Delta \simeq \nu\hbar\omega_{\rm ph}$ since S-phonons are not relevant to the phonon-assisted tunneling between the quantum dots because they couple to the total number of electrons, $n_L + n_R$ in the DQD. The polaron states involving S-phonons are given by

$$|L, n\rangle_{\rm eS} = |L\rangle_{\rm e} \otimes \mathcal{T}_{\rm S}|n\rangle_{\rm S}, \quad |R, n\rangle_{\rm eS} = |R\rangle_{\rm e} \otimes \mathcal{T}_{\rm S}|n\rangle_{\rm S} \tag{28}$$

for an electron in dot L or R, with n phonons, where the lattice distortion

$$\mathcal{T}_{\rm S} = {\rm e}^{-\lambda_{\rm S}(a_{\rm S}^\dagger - a_{\rm S})} \tag{29}$$

is common for $|L, n\rangle_{\rm eS}$ and $|R, n\rangle_{\rm eS}$. S-phonons show neither phonon lasing nor antibunching.

We derive the rate equation for arbitrary level spacing Δ in appendix D. By tracing out S-phonon degrees of freedom, we obtain the reduced rate equation for electrons, which is the same as that in the absence of electron–phonon coupling. We obtain the electric current and electron number in the DQD,

$$I = \frac{e\Gamma_R}{(\Delta/V_{\rm C})^2 + 2 + \gamma}, \quad \langle n_{\rm e} \rangle = \frac{(\Delta/V_{\rm C})^2 + 2}{(\Delta/V_{\rm C})^2 + 2 + \gamma}. \tag{30}$$

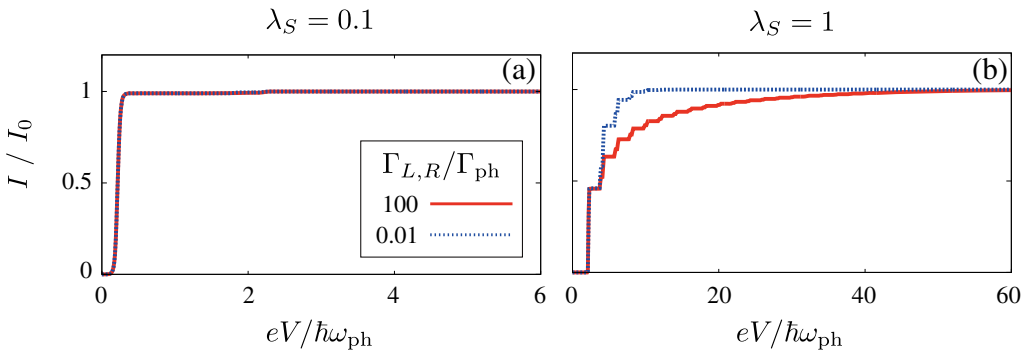

Figure 7. Electric current through the DQD at $\Delta = 0$, as a function of bias voltage V. The dimensionless electron–phonon coupling constants are (a) $\lambda_{\rm S} = 0.1$ or (b) 1, and $\lambda_{\rm A} = 0$. $\Gamma_L = \Gamma_R \equiv \Gamma_{L,R}$, $V_{\rm C} = 0.1\hbar\omega_{\rm ph}$ and $T = 0.01\hbar\omega_{\rm ph}$. Note that two lines almost overlap in (a).

The number of S-phonons is given by

$$\langle N_{\rm S}\rangle = 2\lambda_{\rm S}^2 \frac{I}{e\Gamma_{\rm ph}} + \lambda_{\rm S}^2\langle n_{\rm e}\rangle. \tag{31}$$

The first term in equation (31) indicates the creation of $2\lambda_{\rm S}^2$ phonons by the lattice distortion with two tunnelings between the DQD and leads per single electron transfer through the DQD. The second term describes the average number of polarons. In contrast to equation (22) for A-phonons, S-phonons are not created by the interdot tunneling.

We also examine the autocorrelation function

$$g_{\rm S}^{(2)}(\tau) = \frac{\langle :N_{\rm S}(0)N_{\rm S}(\tau): \rangle}{\langle N_{\rm S}\rangle^2}. \tag{32}$$

$g_{\rm S}^{(2)}(0)$ is independent of $\lambda_{\rm S}$, for arbitrary Δ. When $\Gamma_{L,R}/\Gamma_{\rm ph} \gg 1$, we find

$$g_{\rm S}^{(2)}(0) = 2 + \mathcal{O}(\Gamma_{\rm ph}/\Gamma_{L,R}), \tag{33}$$

which indicates the thermalization induced by the Franck–Condon effect.

4.2. Franck–Condon blockade

Next, we examine the Franck–Condon blockade under finite bias voltages. Figures 7(a) and (b) show the current as a function of V when $\Delta = 0$. The dimensionless coupling constant is (a) $\lambda_{\rm S} = 0.1$ and (b) 1. While the Franck–Condon blockade suppresses the current under small bias voltages in the case of $\lambda_{\rm S} = 1$, the current suppression is negligible in the case of $\lambda_{\rm S} = 0.1$. In the former case, a larger voltage is needed to lift the Franck–Condon blockade for larger $\Gamma_{L,R}/\Gamma_{\rm ph}$.

When $\Gamma_{L,R}/\Gamma_{\rm ph} = 100$, the V dependence of the current is almost the same as in figure 5 for A-phonons with $\Delta = 0$. The phonon number and its autocorrelation function also change with the bias voltage V in a similar manner to those at the current main peak for A-phonons.

5. Coupling with both phonon modes

Now we consider both A- and S-phonons. Here, we examine a DQD fabricated in the semiconductor substrate where an electron is weakly coupled to both phonons; $\lambda_S, \lambda_A \lesssim 0.1$.

First, we analytically derive that the coupling to S-phonons does not influence the calculated results in section 3 for the electron–A-phonon system in the large bias-voltage limit. Consider the current main peak ($\Delta = 0$) and subpeaks ($\Delta = \Delta_\nu \simeq \nu\hbar\omega_{\rm ph}$), assuming that $V_C \ll \hbar\omega_{\rm ph}$. The eigenstates of H are given by the zero-electron states $|0, n; n'\rangle_{eA;S} = |0, n\rangle_{eA} \otimes |n'\rangle_S$, bonding and anti-bonding states between the polarons, $|\pm, n; n'\rangle_{eA;S} = |\pm, n\rangle_{eA} \otimes \mathcal{T}_S|n'\rangle_S$ ($n, n' = 0, 1, 2, \ldots$), and polarons localized in dot R, $|R, n; n'\rangle_{eA;S} = |R, n\rangle_{eA} \otimes \mathcal{T}_S|n'\rangle_S$ ($n = 0, 1, 2, \ldots, \nu$; $n' = 0, 1, 2, \ldots$). The rate equations for these states yield

$$\begin{aligned}\dot{P}_{0,n;n'} = &-\Gamma_L P_{0,n;n'} + \sum_{m,m'=0}^{\infty} \frac{\Gamma_R}{2} |{}_A\langle n|\mathcal{T}_A^\dagger|m+\nu\rangle_A|^2 |{}_S\langle n'|\mathcal{T}_S^\dagger|m'\rangle_S|^2 P_{{\rm mol},m;m'} \\ &+ \sum_{m=0}^{\nu-1}\sum_{m'=0}^{\infty} \Gamma_R |{}_A\langle n|\mathcal{T}_A^\dagger|m\rangle_A|^2 |{}_S\langle n'|\mathcal{T}_S^\dagger|m'\rangle_S|^2 P_{R,m;m'} \\ &+\Gamma_{\rm ph}\left[(n+1)P_{0,n+1;n'} + (n'+1)P_{0,n;n'+1} - (n+n')P_{0,n;n'}\right], \end{aligned} \tag{34}$$

$$\begin{aligned}\dot{P}_{{\rm mol},n;n'} = &-\frac{\Gamma_R}{2} P_{{\rm mol},n;n'} + \sum_{m,m'=0}^{\infty} \Gamma_L |{}_A\langle n|\mathcal{T}_A|m\rangle_A|^2 |{}_S\langle n'|\mathcal{T}_S|m'\rangle_S|^2 P_{0,m;m'} \\ &+\Gamma_{\rm ph}\left[\left(n+1+\frac{\nu}{2}\right)P_{{\rm mol},n+1;n'} + (n'+1)P_{{\rm mol},n;n'+1} - \left(n+n'+\frac{\nu}{2}\right)P_{{\rm mol},n;n'}\right], \end{aligned} \tag{35}$$

where $P_{{\rm mol},n;n'} = P_{+,n;n'} + P_{-,n;n'}$ ($n, n' = 0, 1, 2, \ldots$), and

$$\dot{P}_{R,n;n'} = -\Gamma_R P_{R,n;n'} + \Gamma_{\rm ph}\left[(n+1)P_{R,n+1;n'} + (n'+1)P_{R,n;n'+1} - (n+n')P_{R,n;n'}\right], \tag{36}$$

with $P_{R,\nu;n'} = P_{{\rm mol},0;n'}/2$ ($n = 0, 1, 2, \ldots, \nu-1$; $n' = 0, 1, 2, \ldots$). We trace out S-phonon degrees of freedom by summing up both sides of equations (34)–(36) over n'. We then obtain the reduced rate equations for the electron–A-phonon system, which are just the same as equations (18)–(20) with $P_{0,n} = \sum_{n'=0}^{\infty} P_{0,n;n'}$, $P_{{\rm mol},n} = \sum_{n'} P_{{\rm mol},n;n'}$ and $P_{R,n} = \sum_{n'} P_{R,n;n'}$. This fact indicates that S-phonons do not affect the dynamics of the electron–A-phonon system if the bias voltage is sufficiently large.

In figure 8, we plot (a) the electric current, (b) A- and S-phonon numbers and (c) their autocorrelation function, as a function of Δ, in the case of $\lambda_A = \lambda_S = 0.1$ and $\Gamma_{L,R} \gg \Gamma_{\rm ph}$. The current, phonon number and autocorrelation function for A-phonons are the same as in figure 2 with $\lambda_A = 0.1$ (solid line) where S-phonons are disregarded, in accordance with the above mentioned consideration. An increase in S-phonon number $\langle N_S\rangle$ is induced by the current via the Franck–Condon effect. It is explained by equation (31) using current I and electron number $\langle n_e\rangle$. $g_S^{(2)}(0) \simeq 2$ at the current peaks, indicating the thermalization of S-phonons.

When the bias voltage is finite, S-phonon degrees of freedom cannot be traced out in the rate equation. Therefore, S-phonons can influence the current and distribution of A-phonons. However, the influence is very small, provided that $\lambda_S \sim \lambda_A \lesssim 0.1$, because the

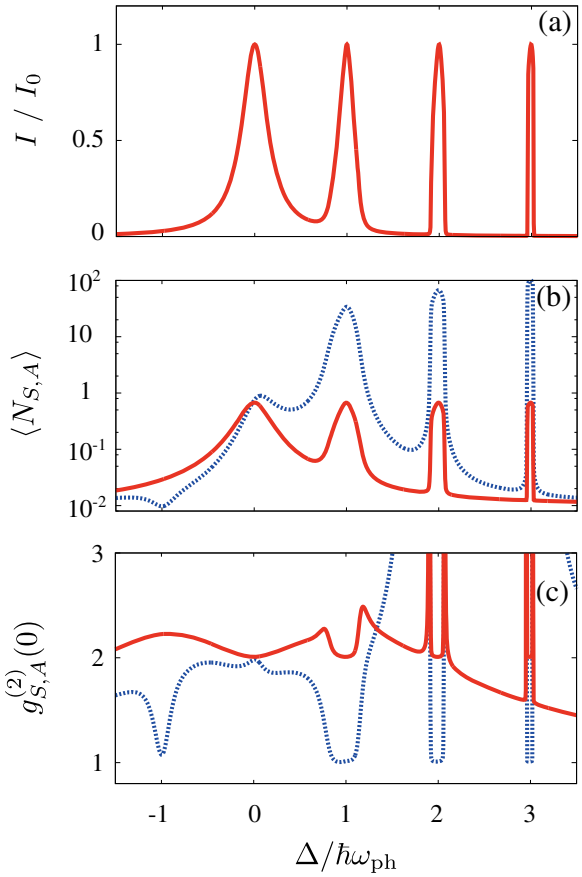

Figure 8. (a) Electric current through the DQD, (b) phonon numbers $\langle N_{\rm S,A}\rangle$ and (c) the autocorrelation function $g^{(2)}_{\rm S,A}(0)$ in the large bias-voltage limit, as a function of level spacing Δ in the DQD. In (b) and (c), data for S-phonons (A-phonons) are indicated by solid (dotted) lines. The dimensionless electron–phonon coupling constants are $\lambda_{\rm A} = \lambda_{\rm S} = 0.1$. In (a), $I_0 = e\Gamma_R/(2 + \Gamma_R/\Gamma_L)$ is the current at $\Delta = 0$ in the absence of electron–phonon coupling. $\Gamma_L = \Gamma_R = 100\,\Gamma_{\rm ph}$ and $V_{\rm C} = 0.1\hbar\omega_{\rm ph}$.

current suppression by the Franck–Condon blockade with S-phonons is negligible, as shown in figure 7(a).

6. Discussion

In this work, we consider single energy levels in quantum dots, ε_L and ε_R ($\Delta = \varepsilon_L - \varepsilon_R$). We take into account the optical phonons, but not the acoustic phonons. When $\Delta \sim \hbar\omega_{\rm ph}$ ($= 36$ meV in GaAs), there are several energy levels in dot R between ε_R and ε_L. Thus, some transport processes should exist in which an electron tunnels from ε_L to excited levels in dot R with emitting LA phonons. These LA-phonon-assisted tunneling processes, however, can be neglected around the current subpeaks at $\Delta = \Delta_\nu$ ($\simeq \nu\hbar\omega_{\rm ph}$) in figure 2(a), where the LO-phonon-assisted tunneling processes are dominant. The reason is as follows. In quantum dots

of radius $\mathcal{R}$, electrons are coupled to acoustic phonons with small wavenumbers of $|\boldsymbol{q}| \lesssim 1/\mathcal{R}$ only[9]. When $\mathcal{R} < 100\,\mathrm{nm}$, the energy of such LA phonons is comparable with or smaller than the level spacing in the quantum dot. Therefore, the number of relevant excited levels in dot R is zero or unity. Besides, the coupling to LA phonons is much weaker than that to LO phonons because of large density of states in the latter. Indeed, the LO-phonon-assisted transport was clearly observed for level spacings Δ tuned to $\hbar\omega_{\mathrm{ph}}$ and $2\hbar\omega_{\mathrm{ph}}$ in recent experiments [18].

Next, we discuss the validity of BMS approximation. BMS approximation is based on the assumption that the typical time scale described by the Hamiltonian, H in equation (7), is much larger than $1/\Gamma_{L,R}$ and $1/\Gamma_{\mathrm{ph}}$ [26]. At the νth current subpeak in semiconductor-based DQDs, the typical time scale is estimated to be $\hbar/W_\nu$ in equation (26). Therefore, our results on the phonon lasing are justified when $V_{\mathrm{C}} \gg \hbar(\Gamma_{L,R}\Gamma_{\mathrm{ph}})^{1/2}/\lambda_{\mathrm{A}}^{\nu}$, and on the phonon antibunching at the first subpeak when $V_{\mathrm{C}} \gg \hbar\Gamma_{\mathrm{ph}}/\lambda_{\mathrm{A}}$. We believe that our results are asymptotically applicable for smaller V_{C}.

Finally, we address the possible experimental realizations to observe LO phonon lasing and antibunching in semiconductor-based DQDs. In GaAs, an LO phonon around the Γ point decays into an LO phonon and a TA phonon around the L point, which are not coupled to the DQD. These daughter phonons can be detected by the transport through another DQD fabricated nearby [31, 32]. Alternatively, the modulation of the dielectric constant by the phonons could be observed by near-field spectroscopy [33]. With a decay rate $\Gamma_{\mathrm{ph}} \sim 0.1\,\mathrm{THz}$ in GaAs [19], however, the lasing condition $\Gamma_{L,R} \gg \Gamma_{\mathrm{ph}}$ might be hard to realize. Other materials with longer lifetime of optical phonons, such as ZnO [34], may be preferable to observe phonon lasing.

7. Conclusions

We have proposed optical phonon lasing in a semiconductor-based DQD under a finite bias voltage, without any requirement of an additional cavity or resonator. First, we have shown that only two phonon modes (S- and A-phonons) are coupled to the DQD, which act as a cavity because of the flat dispersion relation of the optical phonons. The electric transport is accompanied by A-phonon emission when the energy level spacing in the DQD is tuned to the phonon energy. This results in phonon lasing when the tunneling rate $\Gamma_{L,R}$ between the DQD and leads is much larger than phonon decay rate Γ_{ph}. We also find the antibunching of A-phonons in the same system when $\Gamma_{L,R} \lesssim \Gamma_{\mathrm{ph}}$. Both effects are robust against the finite coupling to S-phonons.

For a DQD fabricated in a CNT, we have shown that lasing and antibunching are spoilt by bunched phonons created by the Franck–Condon effect, due to the strong electron–phonon coupling. The coupling also brings about the suppression of the electric current, called Franck–Condon blockade, under finite bias voltages.

Our fundamental research of LO phonon statistics is also applicable to a freestanding semiconductor membrane as a phonon cavity [35, 36], in which a resonating mode plays the role of LO phonons in our theory. Since our theory gives conditions for lasing or antibunching on the electron–phonon coupling and tunneling rate, it would be useful to design a cavity to generate various quantum states. This would lead to new development of nanoelectromechanical systems.

[9] The electron–LA-phonon coupling is described by the piezoelectric or deformation potential. In both cases, the coupling constant involves the integral, $\int \mathrm{d}\boldsymbol{r}|\psi_\alpha(\boldsymbol{r})|^2\,\mathrm{e}^{\mathrm{i}\boldsymbol{q}\cdot\boldsymbol{r}}$, for an electron in dot α and LA phonon with wavenumber $\boldsymbol{q}$, as in the case of electron–LO-phonon coupling in equation (4).

Acknowledgments

The authors acknowledge fruitful discussion with K Ono, S Amaha, Y Kayanuma, K Saito, C Pöltl, T Yokoyama and A Yamada. This work was partially supported by KAKENHI (numbers 23104724 and 24-6574), Institutional Program for Young Researcher Oversea Visits and International Training Program from the Japan Society for the Promotion of Science, Graduate School Doctoral Student Aid Program from Keio University and the German DFG via SFB 910 and project BR 1528/8-1.

Appendix A. Phonon mode function and coupling constant

In this appendix, we derive phonon mode functions, $\boldsymbol{u}_{\mathrm{S}}(\boldsymbol{r})$ and $\boldsymbol{u}_{\mathrm{A}}(\boldsymbol{r})$, shown in figure 1(b). We also estimate the coupling constants $\lambda_{\mathrm{S/A}}$ in equation (8).

Using the optical phonon modes $a_{\boldsymbol{q}}$, the lattice displacement at position $\boldsymbol{r}$ is given by

$$\boldsymbol{u}(\boldsymbol{r}) = -\mathrm{i}\left(\frac{\hbar}{2N\mu\omega_{\mathrm{ph}}}\right)^{1/2}\sum_{\boldsymbol{q}}\frac{\boldsymbol{q}}{q}\mathrm{e}^{\mathrm{i}\boldsymbol{q}\cdot\boldsymbol{r}}(a_{\boldsymbol{q}}+a_{\boldsymbol{q}}^{\dagger}), \tag{A.1}$$

where μ is the reduced mass for a pair of Ga and As atoms in the case of GaAs and N is the number of pairs in the substrate. The mode functions are defined as the coefficients of the S- and A-phonons in the lattice displacement, i.e.

$$\boldsymbol{u}(\boldsymbol{r}) = \boldsymbol{u}_{\mathrm{S}}(\boldsymbol{r})(a_{\mathrm{S}}+a_{\mathrm{S}}^{\dagger}) + \boldsymbol{u}_{\mathrm{A}}(\boldsymbol{r})(a_{\mathrm{A}}+a_{\mathrm{A}}^{\dagger}) + (\text{other modes}). \tag{A.2}$$

From equations (5) and (6), a_{S} and a_{A} are expressed as

$$a_{\mathrm{S/A}} = \frac{\sum_{\boldsymbol{q}}\left(M_{L,\boldsymbol{q}} \pm M_{R,\boldsymbol{q}}\right)a_{\boldsymbol{q}}}{\left(\sum_{\boldsymbol{q}}|M_{L,\boldsymbol{q}} \pm M_{R,\boldsymbol{q}}|^2\right)^{1/2}}. \tag{A.3}$$

Here, we have used

$$\mathcal{S} = \frac{\sum_{\boldsymbol{q}} M_{L,\boldsymbol{q}}M_{R,-\boldsymbol{q}}}{\left(\sum_{\boldsymbol{q}}|M_{L,\boldsymbol{q}}|^2\right)^{1/2}\left(\sum_{\boldsymbol{q}}|M_{R,\boldsymbol{q}}|^2\right)^{1/2}}.$$

From equation (A.3), $a_{\boldsymbol{q}}$ is inversely expanded by a_{S}, a_{A} and other modes:

$$a_{\boldsymbol{q}} = \frac{(M_{L,-\boldsymbol{q}}+M_{R,-\boldsymbol{q}})a_{\mathrm{S}}}{\left(\sum_{\boldsymbol{q}'}|M_{L,\boldsymbol{q}'}+M_{R,\boldsymbol{q}'}|^2\right)^{1/2}} + \frac{(M_{L,-\boldsymbol{q}}-M_{R,-\boldsymbol{q}})a_{\mathrm{A}}}{\left(\sum_{\boldsymbol{q}'}|M_{L,\boldsymbol{q}'}-M_{R,\boldsymbol{q}'}|^2\right)^{1/2}} + \cdots. \tag{A.4}$$

By the substitution of this equation into (A.1), we obtain

$$\begin{aligned}\boldsymbol{u}_{\mathrm{S/A}}(\boldsymbol{r}) &= -\mathrm{i}\left(\frac{\hbar}{2N\mu\omega_{\mathrm{ph}}}\right)^{1/2}\frac{\sum_{\boldsymbol{q}}\frac{\boldsymbol{q}}{q}\mathrm{e}^{\mathrm{i}\boldsymbol{q}\cdot\boldsymbol{r}}(M_{L,-\boldsymbol{q}} \pm M_{R,-\boldsymbol{q}})}{\left(\sum_{\boldsymbol{q}}|M_{L,\boldsymbol{q}} \pm M_{R,\boldsymbol{q}}|^2\right)^{1/2}} \\ &= \left(\frac{\hbar\mathcal{V}}{8\pi N\mu\omega_{\mathrm{ph}}}\right)^{1/2}\frac{1}{C_{\mathrm{S/A}}}\int \mathrm{d}\boldsymbol{r}'\frac{[|\psi_L(\boldsymbol{r}')|^2 \pm |\psi_R(\boldsymbol{r}')|^2](\boldsymbol{r}-\boldsymbol{r}')}{|\boldsymbol{r}-\boldsymbol{r}'|^3}\end{aligned} \tag{A.5}$$

with

$$C_{\mathrm{S/A}}^2 = \int \mathrm{d}\boldsymbol{r}\mathrm{d}\boldsymbol{r}'\frac{\left[|\psi_L(\boldsymbol{r})|^2 \pm |\psi_R(\boldsymbol{r})|^2\right]\left[|\psi_L(\boldsymbol{r}')|^2 \pm |\psi_R(\boldsymbol{r}')|^2\right]}{|\boldsymbol{r}-\boldsymbol{r}'|}. \tag{A.6}$$

In the derivation of equations (A.5) and (A.6), we have used

$$\int \frac{d\boldsymbol{q}}{(2\pi)^3}\frac{1}{q^2}e^{i\boldsymbol{q}\cdot\boldsymbol{r}} = \frac{1}{4\pi|\boldsymbol{r}|}$$

and its gradient with respect to $\boldsymbol{r}$,

$$i\int \frac{d\boldsymbol{q}}{(2\pi)^3}\frac{\boldsymbol{q}}{q^2}e^{i\boldsymbol{q}\cdot\boldsymbol{r}} = -\frac{\boldsymbol{r}}{4\pi|\boldsymbol{r}|^3}.$$

In figure 1(b), we evaluate the mode functions in equation (A.5), assuming spherical Gaussian functions of radius $\mathcal{R}$ for the electron distribution in the quantum dots, $|\psi_L(\boldsymbol{r})|^2$ and $|\psi_R(\boldsymbol{r})|^2$.

The coupling constants $\lambda_{S/A}$ in equation (8) are written as

$$\lambda_{S/A}^2 = \frac{e^2}{32\pi\hbar\omega_{ph}}\left[\frac{1}{\epsilon(\infty)} - \frac{1}{\epsilon(0)}\right]C_{S/A}^2 \tag{A.7}$$

with $C_{S/A}$ in equation (A.6). Using the spherical Gaussian functions for $|\psi_L(\boldsymbol{r})|^2$ and $|\psi_R(\boldsymbol{r})|^2$, we find

$$\lambda_{S/A}^2 \simeq \frac{1}{\sqrt{32\pi^3}}\left[\frac{1}{\epsilon(\infty)} - \frac{1}{\epsilon(0)}\right]\left(1 \pm \sqrt{\frac{\pi}{2}}\frac{\mathcal{R}}{d}\right)\frac{e^2}{\hbar\omega_{ph}\mathcal{R}}, \tag{A.8}$$

where $d = |\boldsymbol{r}_{LR}|$ is the distance between centers of the two quantum dots. This yields $\lambda_{S/A} = 0.01$–0.1 for $\mathcal{R} = 100$–10 nm and $d \gtrsim 2\mathcal{R}$, in the case of GaAs.

Appendix B. Effective Hamiltonian for double quantum dot in carbon nanotube

In this appendix, we derive the effective Hamiltonian for a DQD embedded in a suspended CNT. An electron in the CNT is strongly coupled to the longitudinal stretching modes of phonons, known as vibrons, by the deformation potential [37]. We assume that quantum dots L and R are fabricated around $x = x_L$ and x_R, respectively, in $0 < x < \ell$ along the CNT. The phonon-related parts of the Hamiltonian are given by

$$\mathcal{H}_{ph} = \sum_{n=1}^{\infty}\hbar\omega_n a_n^\dagger a_n, \tag{B.1}$$

$$\mathcal{H}_{ep} = \sum_{\alpha=L,R}\sum_{n=1}^{\infty}\lambda_{\alpha,n}\hbar\omega_n(a_n + a_n^\dagger)n_\alpha, \tag{B.2}$$

where a_n ($a_n^\dagger$) is the annihilation (creation) operator for the phonon with wavenumber $q_n = n\pi/\ell$ ($n = 1, 2, 3, \ldots$). The phonon energy is given by

$$\hbar\omega_n = \hbar v q_n = n\frac{\pi\hbar v}{\ell} \tag{B.3}$$

using sound velocity v, for small n. The dimensionless coupling constants are

$$\lambda_{\alpha,n} \simeq \frac{3}{\sqrt{n(\ell_\perp/\mathrm{nm})}}\cos(q_n x_\alpha) \tag{B.4}$$

with $(\ell_\perp/\mathrm{nm})$ being the circumference of the CNT in units of nanometer [37]. When x_L and x_R are symmetric with respect to $x = \ell/2$, $\lambda_{L,1} = -\lambda_{R,1}$. Disregarding the higher modes of $n \geqslant 2$, we obtain the effective Hamiltonian in equation (7) with $a_\mathrm{A} = a_1$, $\hbar\omega_\mathrm{ph} = \hbar\omega_1$, $\lambda_\mathrm{A} = \lambda_{L,1}$ and $\lambda_\mathrm{S} = 0$.

Appendix C. Analytic expression for A-phonon distribution at current peaks

In this appendix, we derive the analytical expressions for the current I, number of phonons $\langle N_\mathrm{A}\rangle$ and autocorrelation function of phonons $g_\mathrm{A}^{(2)}(0)$ in equations (21)–(24) when the level spacing Δ is tuned to the current subpeaks in figure 2; $\Delta = \Delta_\nu (\simeq \nu\hbar\omega_\mathrm{ph})$. We assume that $\lambda_\mathrm{S} = 0$ and consider the large bias-voltage limit. The energy eigenstates are given by the zero-electron states $|0, n\rangle_\mathrm{eA} = |0\rangle_\mathrm{e} \otimes |n\rangle_\mathrm{A}$, bonding and anti-bonding states between the polarons $|\pm, n\rangle_\mathrm{eA} = \frac{1}{\sqrt{2}}\left(|L, n\rangle_\mathrm{eA} \pm |R, n+\nu\rangle_\mathrm{eA}\right)$, and polarons localized in dot R, $|R, n\rangle_\mathrm{eA}$ $(n = 0, 1, 2, \ldots, \nu - 1)$, in a good approximation for $V_\mathrm{C} \ll \hbar\omega_\mathrm{ph}$, as mentioned in section 3. $|L, n\rangle_\mathrm{eA}$ and $|R, n\rangle_\mathrm{eA}$ are given in equation (15). The density matrix is given by

$$\rho_\mathrm{eA} = \sum_{n=0}^{\infty} P_{0,n} |0, n\rangle_{\mathrm{eA}\ \mathrm{eA}}\langle 0, n| + \sum_{\sigma=\pm}\sum_{n=0}^{\infty} P_{\sigma,n} |\sigma, n\rangle_{\mathrm{eA}\ \mathrm{eA}}\langle \sigma, n| + \sum_{n=0}^{\nu-1} P_{R,n} |R, n\rangle_{\mathrm{eA}\ \mathrm{eA}}\langle R, n|$$

in the BMS approximation. The occupation numbers for zero-electron states, n_0, bonding or anti-bonding states between the polarons, n_mol, and polarons localized in dot R, n_R, are given by

$$n_0 = \sum_{n=0}^{\infty} |0, n\rangle_{\mathrm{eA}\ \mathrm{eA}}\langle 0, n| = |0\rangle_{\mathrm{e}\ \mathrm{e}}\langle 0|,$$

$$n_\mathrm{mol} = \sum_{\sigma=\pm}\sum_{n=0}^{\infty} |\sigma, n\rangle_{\mathrm{eA}\ \mathrm{eA}}\langle \sigma, n|,$$

$$\tilde{n}_R = \sum_{n=0}^{\nu-1} |R, n\rangle_{\mathrm{eA}\ \mathrm{eA}}\langle R, n|,$$

respectively. They satisfy the relation of $n_0 + n_\mathrm{mol} + \tilde{n}_R = 1$. The electron number in the DQD is given by $n_\mathrm{e} = n_\mathrm{mol} + \tilde{n}_R = 1 - n_0$. The expectation values of these occupation numbers are expressed as

$$\langle n_0\rangle = \sum_{n=0}^{\infty} P_{0,n}, \quad \langle n_\mathrm{mol}\rangle = \sum_{n=0}^{\infty} P_{\mathrm{mol},n}, \quad \langle \tilde{n}_R\rangle = \sum_{n=0}^{\nu-1} P_{R,n}.$$

In the stationary state, equations (18)–(20) yield

$$0 = -\Gamma_L P_{0,n} + \sum_{m=0}^{\infty} \frac{\Gamma_R}{2} |_\mathrm{A}\langle n|\mathcal{T}_\mathrm{A}^\dagger|m+\nu\rangle_\mathrm{A}|^2 P_{\mathrm{mol},m} + \sum_{m=0}^{\nu-1} \Gamma_R |_\mathrm{A}\langle n|\mathcal{T}_\mathrm{A}^\dagger|m\rangle_\mathrm{A}|^2 P_{R,m}$$
$$+\Gamma_\mathrm{ph}\left[(n+1)P_{0,n+1} - nP_{0,n}\right], \tag{C.1}$$

$$0 = -\frac{\Gamma_R}{2} P_{\mathrm{mol},n} + \sum_{m=0}^{\infty} \Gamma_L |{}_{\mathrm{A}}\langle n|\mathcal{T}_{\mathrm{A}}|m\rangle_{\mathrm{A}}|^2 P_{0,m} + \Gamma_{\mathrm{ph}} \left[\left(n+1+\frac{\nu}{2} \right) P_{\mathrm{mol},n+1} - \left(n+\frac{\nu}{2} \right) P_{\mathrm{mol},n} \right] \quad \text{(C.2)}$$

with $P_{\mathrm{mol},n} = P_{+,n} + P_{-,n}$ $(n = 0, 1, 2, \ldots)$, and

$$0 = -\Gamma_R P_{R,n} + \Gamma_{\mathrm{ph}} \left[(n+1) P_{R,n+1} - n P_{R,n} \right] \quad \text{(C.3)}$$

with $P_{R,\nu} = P_{\mathrm{mol},0}/2$ $(n = 0, 1, 2, \ldots, \nu - 1)$.

C.1. Current and electron number

First, we calculate the current $I = e\Gamma_L \langle n_0 \rangle$. For the purpose, we sum up both sides of equation (C.1) over n. Using

$$\sum_{n=0}^{\infty} |{}_{\mathrm{A}}\langle n|\mathcal{T}_{\mathrm{A}}^{\dagger}|m\rangle_{\mathrm{A}}|^2 = {}_{\mathrm{A}}\langle m|\mathcal{T}_{\mathrm{A}} \left(\sum_n |n\rangle_{\mathrm{AA}}\langle n| \right) \mathcal{T}_{\mathrm{A}}^{\dagger}|m\rangle_{\mathrm{A}} = 1,$$

we obtain

$$0 = -\Gamma_L \langle n_0 \rangle + \frac{\Gamma_R}{2} \langle n_{\mathrm{mol}} \rangle + \Gamma_R \langle \tilde{n}_R \rangle.$$

Since $\langle n_0 \rangle + \langle n_{\mathrm{mol}} \rangle + \langle \tilde{n}_R \rangle = 1$, we obtain

$$\langle n_0 \rangle = \frac{\gamma}{2+\gamma}(1 + \langle \tilde{n}_R \rangle), \quad \langle n_{\mathrm{mol}} \rangle = \frac{2}{2+\gamma} \left[1 - (1+\gamma)\langle \tilde{n}_R \rangle \right],$$

where $\gamma = \Gamma_R / \Gamma_L$. These equations result in equation (21), i.e.

$$I = e\Gamma_R \frac{1 + \langle \tilde{n}_R \rangle}{2+\gamma}, \quad \langle n_{\mathrm{e}} \rangle = \frac{2 - \gamma \langle \tilde{n}_R \rangle}{2+\gamma}.$$

The summation of equation (C.3) over n yields

$$\langle \tilde{n}_R \rangle = \frac{\nu \Gamma_{\mathrm{ph}}}{2\Gamma_R} P_{\mathrm{mol},0}. \quad \text{(C.4)}$$

C.2. Phonon number

Next, we derive the phonon number

$$\begin{aligned} \langle N_{\mathrm{A}} \rangle &= \sum_{n=0}^{\infty} P_{0,n}\, {}_{\mathrm{eA}}\langle 0, n|N_{\mathrm{A}}|0, n\rangle_{\mathrm{eA}} + \sum_{\sigma=\pm} \sum_{n=0}^{\infty} P_{\sigma,n}\, {}_{\mathrm{eA}}\langle \sigma, n|N_{\mathrm{A}}|\sigma, n\rangle_{\mathrm{eA}} + \sum_{n=0}^{\nu-1} P_{R,n}\, {}_{\mathrm{eA}}\langle R, n|N_{\mathrm{A}}|R, n\rangle_{\mathrm{eA}} \\ &= \sum_{n=0}^{\infty} n P_{0,n} + \sum_{n=0}^{\infty} \left(n + \frac{\nu}{2} + \lambda_{\mathrm{A}}^2 \right) P_{\mathrm{mol},n} + \sum_{n=0}^{\nu-1} (n + \lambda_{\mathrm{A}}^2) P_{R,n} \\ &\equiv \langle N_{\mathrm{A}} n_0 \rangle + \langle N_{\mathrm{A}} n_{\mathrm{mol}} \rangle + \langle N_{\mathrm{A}} \tilde{n}_R \rangle. \end{aligned}$$

We have used the relation, $\mathcal{T}_{\mathrm{A}}^{\dagger} N_{\mathrm{A}} \mathcal{T}_{\mathrm{A}} = (\mathcal{T}_{\mathrm{A}}^{\dagger} a_{\mathrm{A}}^{\dagger} \mathcal{T}_{\mathrm{A}})(\mathcal{T}_{\mathrm{A}}^{\dagger} a_{\mathrm{A}} \mathcal{T}_{\mathrm{A}}) = (a_{\mathrm{A}}^{\dagger} - \lambda_{\mathrm{A}})(a_{\mathrm{A}} - \lambda_{\mathrm{A}})$. We multiply both sides of equations (C.1)–(C.3) by n and sum up over n. Then we find

$$0 = -(\Gamma_L + \Gamma_{\mathrm{ph}}) \langle N_{\mathrm{A}} n_0 \rangle + \frac{\Gamma_R}{2} \langle N_{\mathrm{A}} n_{\mathrm{mol}} \rangle + \Gamma_R \langle N_{\mathrm{A}} \tilde{n}_R \rangle + \frac{\nu \Gamma_R}{4} \langle n_{\mathrm{mol}} \rangle, \quad \text{(C.5)}$$

$$0=\Gamma_L\langle N_{\rm A}n_0\rangle-\left(\frac{\Gamma_R}{2}+\Gamma_{\rm ph}\right)\langle N_{\rm A}n_{\rm mol}\rangle+\lambda_{\rm A}^2\Gamma_L\langle n_0\rangle+\left(\frac{\nu+2\lambda_{\rm A}^2}{4}\Gamma_R+\lambda_{\rm A}^2\Gamma_{\rm ph}\right)\langle n_{\rm mol}\rangle+\Gamma_R\langle\tilde{n}_R\rangle, \tag{C.6}$$

$$0=-(\Gamma_R+\Gamma_{\rm ph})\langle N_{\rm A}\tilde{n}_R\rangle+\left[(\nu-1+\lambda_{\rm A}^2)\Gamma_R+\lambda_{\rm A}^2\Gamma_{\rm ph}\right]\langle\tilde{n}_R\rangle. \tag{C.7}$$

Here, we have used

$$\sum_{n=0}^{\infty}n|_{\rm A}\langle n|\mathcal{T}_{\rm A}^{\dagger}|m\rangle_{\rm A}|^2=_{\rm A}\langle m|\mathcal{T}_{\rm A}N_{\rm A}\left(\sum_n|n\rangle_{\rm AA}\langle n|\right)\mathcal{T}_{\rm A}^{\dagger}|m\rangle_{\rm A}=\sum_m{}_{\rm A}\langle m|\mathcal{T}_{\rm A}N_{\rm A}\mathcal{T}_{\rm A}^{\dagger}|m\rangle_{\rm A}. \tag{C.8}$$

From equations (C.5)–(C.7), we obtain equation (22), i.e.

$$\langle N_{\rm A}\rangle=(\nu+2\lambda_{\rm A}^2)\frac{I}{e\Gamma_{\rm ph}}+\lambda_{\rm A}^2\langle n_{\rm e}\rangle.$$

C.3. Phonon autocorrelation function

Finally, we derive the phonon autocorrelation function at $\tau=0$,

$$g_{\rm A}^{(2)}(0)=\frac{\langle:N_{\rm A}^2:\rangle}{\langle N_{\rm A}\rangle^2}=\frac{\langle N_{\rm A}^2\rangle-\langle N_{\rm A}\rangle}{\langle N_{\rm A}\rangle^2},$$

where

$$\begin{aligned}\langle N_{\rm A}^2\rangle=&\sum_{n=0}^{\infty}P_{0,n}\,{}_{\rm eA}\langle 0,n|N_{\rm A}^2|0,n\rangle_{\rm eA}+\sum_{\sigma=\pm}\sum_{n=0}^{\infty}P_{\sigma,n}\,{}_{\rm eA}\langle\sigma,n|N_{\rm A}^2|\sigma,n\rangle_{\rm eA}+\sum_{n=0}^{\nu-1}P_{R,n}\,{}_{\rm eA}\langle R,n|N_{\rm A}^2|R,n\rangle_{\rm eA}\\&=\sum_{n=0}^{\infty}n^2P_{0,n}+\sum_{n=0}^{\infty}\left[n^2+\lambda_{\rm A}^2(4n+1+\lambda_{\rm A}^2)+\nu\left(n+\frac{\nu}{2}+2\lambda_{\rm A}^2\right)\right]P_{\rm mol,n}\\&\quad+\sum_{n=0}^{\nu-1}\left[n^2+\lambda_{\rm A}^2(4n+1+\lambda_{\rm A}^2)\right]P_{R,n}\\&\equiv\langle N_{\rm A}^2n_0\rangle+\langle N_{\rm A}^2n_{\rm mol}\rangle+\langle N_{\rm A}^2\tilde{n}_R\rangle.\end{aligned}$$

We multiply both sides of equations (C.1)–(C.3) by n^2 and sum up over n. A similar technique to equation (C.8) leads to

$$\begin{aligned}0=&-(\Gamma_L+2\Gamma_{\rm ph})\langle N_{\rm A}^2n_0\rangle+\frac{\Gamma_R}{2}\langle N_{\rm A}^2n_{\rm mol}\rangle+\Gamma_R\langle N_{\rm A}^2\tilde{n}_R\rangle+\Gamma_{\rm ph}\langle N_{\rm A}n_0\rangle\\&+\frac{\nu\Gamma_R}{2}\langle N_{\rm A}n_{\rm mol}\rangle+\frac{\nu\lambda_{\rm A}^2\Gamma_R}{2}\langle n_{\rm mol}\rangle,\end{aligned} \tag{C.9}$$

$$\begin{aligned}0=&\Gamma_L\langle N_{\rm A}^2n_0\rangle-\left(\frac{\Gamma_R}{2}+2\Gamma_{\rm ph}\right)\langle N_{\rm A}^2n_{\rm mol}\rangle+4\lambda_{\rm A}^2\Gamma_L\langle N_{\rm A}n_0\rangle\\&+\left[\frac{\nu+4\lambda_{\rm A}^2}{2}\Gamma_R+(\nu+1+8\lambda_{\rm A}^2)\Gamma_{\rm ph}\right]\langle N_{\rm A}n_{\rm mol}\rangle\lambda_{\rm A}^2(1+\lambda_{\rm A}^2)\Gamma_L\langle n_0\rangle\\&+\lambda_{\rm A}^2\left[\frac{1-\nu-3\lambda_{\rm A}^2}{2}\Gamma_R+(1-\nu-6\lambda_{\rm A}^2)\Gamma_{\rm ph}\right]\langle n_{\rm mol}\rangle-\Gamma_R\langle\tilde{n}_R\rangle,\end{aligned} \tag{C.10}$$

$$0 = -(\Gamma_R + 2\Gamma_{\rm ph})\langle N_{\rm A}^2 \tilde{n}_R\rangle + \left[4\lambda_{\rm A}^2\Gamma_R + (1+8\lambda_{\rm A}^2)\Gamma_{\rm ph}\right]\langle N_{\rm A}\tilde{n}_R\rangle + \left\{\left[(\nu-1)^2 + \lambda_{\rm A}^2(1-3\lambda_{\rm A}^2)\right]\Gamma_R + \lambda_{\rm A}^2(1-6\lambda_{\rm A}^2)\Gamma_{\rm ph}\right\}\langle \tilde{n}_R\rangle. \tag{C.11}$$

From equations (C.9)–(C.11), we find

$$\langle N_{\rm A}^2\rangle - \langle N_{\rm A}\rangle = 2\lambda_{\rm A}^2\frac{\Gamma_L}{\Gamma_{\rm ph}}\langle N_{\rm A} n_0\rangle + \left(\frac{\nu+2\lambda_{\rm A}^2}{2}\frac{\Gamma_R}{\Gamma_{\rm ph}} + \frac{\nu+4\lambda_{\rm A}^2}{2}\right)\langle N_{\rm A} n_{\rm mol}\rangle + 2\lambda_{\rm A}^2\left(\frac{\Gamma_R}{\Gamma_{\rm ph}}+2\right)\langle N_{\rm A}\tilde{n}_R\rangle - \frac{\nu+2\lambda_{\rm A}^4}{2}\frac{\Gamma_L}{\Gamma_{\rm ph}}\langle n_0\rangle - \frac{\lambda_{\rm A}^2(\nu+6\lambda_{\rm A}^2)}{2}\langle n_{\rm mol}\rangle - \left[\frac{\nu(2-\nu)}{2}\frac{\Gamma_R}{\Gamma_{\rm ph}} + 3\lambda_{\rm A}^2\right]\langle \tilde{n}_R\rangle.$$

Now we evaluate $g_{\rm A}^{(2)}(0)$ when $\Gamma_{L,R} \gg \Gamma_{\rm ph}$. In this case, $\langle \tilde{n}_R\rangle = \mathcal{O}(\Gamma_{\rm ph}/\Gamma_{L,R})$ from equation (C.4). Then

$$I = \frac{e\Gamma_R}{2+\gamma} + \mathcal{O}(\Gamma_{\rm ph}/\Gamma_{L,R}), \quad \langle N_{\rm A}\rangle = \frac{\nu+2\lambda_{\rm A}^2}{2+\gamma}\frac{\Gamma_R}{\Gamma_{\rm ph}} + \mathcal{O}(1).$$

Equations (C.5) and (C.7) yield

$$2\langle N_{\rm A} n_0\rangle = \gamma\langle N_{\rm A} n_{\rm mol}\rangle + \mathcal{O}(1), \quad \langle N_{\rm A}\tilde{n}_R\rangle = \mathcal{O}(\Gamma_{\rm ph}/\Gamma_{L,R}).$$

Using $\langle N_{\rm A}\rangle = \langle N_{\rm A} n_0\rangle + \langle N_{\rm A} n_{\rm mol}\rangle + \langle N_{\rm A}\tilde{n}_R\rangle$, we have

$$\langle N_{\rm A} n_0\rangle = (\nu+2\lambda_{\rm A}^2)\frac{\gamma}{(2+\gamma)^2}\frac{\Gamma_R}{\Gamma_{\rm ph}} + \mathcal{O}(1),$$

$$\langle N_{\rm A} n_{\rm mol}\rangle = (\nu+2\lambda_{\rm A}^2)\frac{2}{(2+\gamma)^2}\frac{\Gamma_R}{\Gamma_{\rm ph}} + \mathcal{O}(1).$$

Using these relations, we obtain equation (24), i.e.

$$g_{\rm A}^{(2)}(0) = \frac{\nu+4\lambda_{\rm A}^2}{\nu+2\lambda_{\rm A}} + \mathcal{O}(\Gamma_{\rm ph}/\Gamma_{L,R}).$$

C.4. Case of large decay rate of phonon

Here, we comment on the opposite limit of $\Gamma_{L,R} \ll \Gamma_{\rm ph}$. The analytical expressions for the current, $g_{\rm A}^{(2)}(0)$, etc can be obtained in a similar way to the case of $\Gamma_{L,R} \gg \Gamma_{\rm ph}$. At the main peak of the current ($\Delta = 0$), the electron number and current are written as

$$\langle n_{\rm e}\rangle = \langle n_{\rm mol}\rangle \simeq \frac{1}{2+\gamma}, \quad I \simeq \frac{e\Gamma_R}{2+\gamma},$$

whereas the phonon number and its autocorrelation function are

$$\langle N_{\rm A}\rangle \simeq \frac{\lambda_{\rm A}^2}{2+\gamma}, \quad g_{\rm A}^{(2)}(0) \simeq 2+\gamma.$$

At the νth subpeak of the current ($\Delta = \Delta_\nu \simeq \nu\hbar\omega_{\rm ph}$), we obtain

$$\langle n_{\rm e}\rangle \simeq \langle \tilde{n}_R\rangle \simeq \frac{1}{1+\gamma}, \quad \langle n_{\rm mol}\rangle \simeq 0, \quad I \simeq \frac{e\Gamma_R}{1+\gamma}$$

and

$$\langle N_{\rm A}\rangle \simeq \frac{\lambda_{\rm A}^2}{1+\gamma}, \quad g_{\rm A}^{(2)}(0) \simeq 1+\gamma. \tag{C.12}$$

As discussed in section 3.4, phonon bunching is observed even for small λ_A in the case of $\Gamma_{L,R} \ll \Gamma_{ph}$. In this case, an electron is localized in dot R for a long time, forming a polaron $|R, 0\rangle_{eA}$, after a phonon is immediately decayed. Thus, the number of phonons created by the interdot tunneling is much smaller than that accompanied by the polaron staying in dot R. This situation results in the bunched phonons.

Appendix D. Rate equation for S-phonon

In this appendix, we derive the rate equation in the presence of S-phonons only ($\lambda_A = 0$). We can analytically diagonalize Hamiltonian H for any Δ in this case. The eigenstates of H are given by the zero-electron states, $|0, n\rangle_{eS} = |0\rangle_e \otimes |n\rangle_S$, and bonding and anti-bonding states between the polarons

$$|+, n\rangle_{eS} = \cos\frac{\theta}{2}|L, n\rangle_{eS} + \sin\frac{\theta}{2}|R, n\rangle_{eS}, \tag{D.1}$$

$$|-, n\rangle_{eS} = -\sin\frac{\theta}{2}|L, n\rangle_{eS} + \cos\frac{\theta}{2}|R, n\rangle_{eS} \tag{D.2}$$

with $\tan\theta = 2V_C/\Delta$. $|L, n\rangle_{eS}$ and $|R, n\rangle_{eS}$ are given in equation (28). The corresponding energy eigenvalues are $\epsilon_{0,n} = n\hbar\omega_{ph}$ and

$$\epsilon_{\pm,n} = \pm\left[(\Delta/2)^2 + V_C^2\right]^{1/2} + (n - \lambda_S^2)\hbar\omega_{ph}$$

($n = 0, 1, 2, \ldots$), respectively. Using the dissipator $\mathcal{L}_e$ in equation (10), we obtain the rate equations under a finite bias voltage as

$$\dot{P}_{0,n} = -\left[\sum_{\alpha=L,R}\sum_{\sigma=\pm}\sum_{m=0}^{\infty} f_\alpha(\epsilon_{\sigma,m} - \epsilon_{0,n})\Gamma_{\alpha,\sigma}|_S\langle m|\mathcal{T}_S^\dagger|n\rangle_S|^2\right]P_{0,n}$$
$$+\sum_{\alpha,\sigma,m}\bar{f}_\alpha(\epsilon_{\sigma,m} - \epsilon_{0,n})\Gamma_{\alpha,\sigma}|_S\langle n|\mathcal{T}_S|m\rangle_S|^2 P_{\sigma,m} + \Gamma_{ph}\left[(n+1)P_{0,n+1} - nP_{0,n}\right], \tag{D.3}$$

$$\dot{P}_{\pm,n} = -\left[\sum_{\alpha,m}\bar{f}_\alpha(\epsilon_{\pm,n} - \epsilon_{0,m})\Gamma_{\alpha,\pm}|_S\langle m|\mathcal{T}_S|n\rangle_S|^2\right]P_{\pm,n}$$
$$+\sum_{\alpha,m} f_\alpha(\epsilon_{\pm,n} - \epsilon_{0,m})\Gamma_{\alpha,\pm}|_S\langle n|\mathcal{T}_S^\dagger|m\rangle_S|^2 P_{0,m} + \Gamma_{ph}\left[(n+1)P_{\pm,n+1} - nP_{\pm,n}\right]. \tag{D.4}$$

Here, we have introduced tunnel coupling strength $\Gamma_{\alpha,\sigma}$ between lead α and molecule orbital σ in equations (D.1) and (D.2): $\Gamma_{L,+} = \Gamma_L\cos^2(\theta/2)$, $\Gamma_{L,-} = \Gamma_L\sin^2(\theta/2)$, $\Gamma_{R,+} = \Gamma_R\sin^2(\theta/2)$ and $\Gamma_{R,-} = \Gamma_R\cos^2(\theta/2)$. In the limit of large bias, these equations yield

$$\dot{P}_{0,n} = -\Gamma_L P_{0,n} + \sum_{\sigma=\pm}\sum_{m=0}^{\infty}\Gamma_{R,\sigma}|_S\langle n|\mathcal{T}_S|m\rangle_S|^2 P_{\sigma,m} + \Gamma_{ph}\left[(n+1)P_{0,n+1} - nP_{0,n}\right], \tag{D.5}$$

$$\dot{P}_{\pm,n} = -\Gamma_{R,\pm}P_{\pm,n} + \sum_{m=0}^{\infty}\Gamma_{L,\pm}|_S\langle n|\mathcal{T}_S^\dagger|m\rangle_S|^2 P_{0,m} + \Gamma_{ph}\left[(n+1)P_{\pm,n+1} - nP_{\pm,n}\right]. \tag{D.6}$$

We sum up both sides of equations (D.5) and (D.6) over n to obtain the reduced rate equations for electrons

$$\dot{P}_0 = -\Gamma_L P_0 + \sum_{\sigma=\pm} \Gamma_{R,\sigma} P_\sigma, \tag{D.7}$$

$$\dot{P}_\pm = -\Gamma_{R,\pm} P_\pm + \Gamma_{L,\pm} P_0 \tag{D.8}$$

with $P_0 = \sum_{n=0}^{\infty} P_{0,n}$ and $P_\pm = \sum_n P_{\pm,n}$. Equations (D.7) and (D.8) are the same as those in the absence of electron–phonon coupling. This indicates that S-phonons do not affect the electron transfer in the large bias-voltage limit, whereas they are created by the current through the Franck–Condon effect. Further calculation yields the current, electron and S-phonon numbers and phonon autocorrelation function in equations (30), (31) and (33), in a similar way to appendix C.

References

[1] McKeever J, Boca A, Boozer A D, Buck J R and Kimble H J 2003 *Nature* **425** 268
[2] Walther H, Varcoe B T H, Englert B-G and Becker T 2006 *Rep. Prog. Phys.* **69** 1325
[3] Choi W, Lee J-H, An K, Fang-Yen C, Dasari R R and Feld M S 2006 *Phys. Rev. Lett.* **96** 093603
[4] Hennessy K, Badolato A, Winger M, Gerace D, Atatüre M, Gulde S, Fält S, Hu E L and Imamoğlu A 2007 *Nature* **445** 896
[5] Bozyigit D *et al* 2011 *Nature Phys.* **7** 154
[6] Astafiev O, Inomata K, Niskanen A O, Yamamoto T, Pashkin Y A, Nakamura Y and Tsai J S 2007 *Nature* **449** 588
[7] Blais A, Huang R S, Wallraff A, Girvin S M and Schoelkopf R J 2004 *Phys. Rev.* A **69** 062320
[8] Ashhab S, Johansson J R, Zagoskin A M and Nori F 2009 *New J. Phys.* **11** 023030
[9] André S, Brosco V, Shnirman A and Schön G 2009 *Phys. Rev.* A **79** 053848
[10] Gartner P 2011 *Phys. Rev.* A **84** 053804
[11] Xiang Z-L, Ashhab S, You J Q and Nori F 2013 *Rev. Mod. Phys.* **85** 623
[12] Roulleau P, Baer S, Choi T, Molitor F, Güttinger J, Müller T, Dröscher S, Ensslin K and Ihn T 2011 *Nature Commun.* **2** 239
[13] Brandes T and Kramer B 1999 *Phys. Rev. Lett.* **83** 3021
[14] Sapmaz S, Jarillo-Herrero P, Blanter Y M, Dekker C and van der Zant H S J 2006 *Phys. Rev. Lett.* **96** 026801
[15] Leturcq R, Stampfer C, Inderbitzin K, Durrer L, Hierold C, Mariani E, Schultz M G, von Oppen F and Ensslin K 2009 *Nature Phys.* **5** 327
[16] Koch J and von Oppen F 2005 *Phys. Rev. Lett.* **94** 206804
[17] Atkins P and Friedman R 2005 *Molecular Quantum Mechanics* (Oxford: Oxford University Press)
[18] Amaha S and Ono K 2012 private communications
[19] Vallée F 1994 *Phys. Rev.* B **49** 2460
[20] Okuyama R, Eto M and Brandes T 2013 *J. Phys. Soc. Japan* **82** 013704
[21] Gnodtke C, Kießlich G, Schöll E and Wacker A 2006 *Phys. Rev.* B **73** 115338
[22] Beardsley R P, Akimov A V, Henini M and Kent A J 2010 *Phys. Rev. Lett.* **104** 085501
[23] Kabuss J, Carmele A, Brandes T and Knorr A 2012 *Phys. Rev. Lett.* **109** 054301
[24] Khaetskii A, Golovach V N, Hu X and Žutić I 2013 arXiv:1306.1786
[25] Hübener H and Brandes T 2009 *Phys. Rev.* B **80** 155437
[26] Breuer H P and Petruccione F 2002 *The Theory of Open Quantum Systems* (Oxford: Oxford University Press)
[27] Hameau S, Guldner Y, Verzelen O, Ferreira R, Bastard G, Zeman J, Lemaître A and Gérard J M 1999 *Phys. Rev. Lett.* **83** 4152
[28] Scully M O and Zubairy M S 1997 *Quantum Optics* (Cambridge: Cambridge University Press)

[29] Emary C, Pöltl C, Carmele A, Kabuss J, Knorr A and Brandes T 2012 *Phys. Rev.* B **85** 165417
[30] Lambert N and Nori F 2008 *Phys. Rev.* B **78** 214302
[31] Gasser U, Gustavsson S, Küng B, Ensslin K, Ihn T, Driscoll D C and Gossard A C 2009 *Phys. Rev.* B **79** 035303
[32] Harbusch D, Taubert D, Tranitz H P, Wegscheider W and Ludwig S 2010 *Phys. Rev. Lett.* **104** 196801
[33] Cunningham J, Byrne M, Upadya P, Lachab M, Linfield E H and Davies A G 2008 *Appl. Phys. Lett.* **92** 032903
[34] Aku-Leh C, Zhao J, Merlin R, Menéndez J and Cardona M 2005 *Phys. Rev.* B **71** 205211
[35] Weig E M, Blick R H, Brandes T, Kirschbaum J, Wegscheider W, Bichler M and Kotthaus J P 2004 *Phys. Rev. Lett.* **92** 046804
[36] Ogi J, Ferrus T, Kodera T, Tsuchiya Y, Uchida K, Williams D A, Oda S and Mizuta H 2010 *Japan. J. Appl. Phys.* **49** 045203
[37] Mariani E and von Oppen F 2009 *Phys. Rev.* B **80** 155411